Plant Physiology®

Plant Physiology, 2024, 00, 1–19
https://doi.org/10.1093/plphys/kiae383
Advance access publication 25 July 2024
Research Article

Abscisic acid–mediated autoregulation of the MYB41-BRAHMA module enhances drought tolerance in Arabidopsis

Lei Gao,[1,†] Qiang Lv,[1,*†] Lei Wang,[1,2,*†‡] Shuang Han,[1,†] Jing Wang,[1] Yuli Chen,[1] Wenwen Zhu,[1] Xia Zhang,[1] Fang Bao,[1] Yong Hu,[1] Ling Li,[2,*] Yikun He[1,*]

[1]College of Life Sciences, Capital Normal University, Beijing 100048, China
[2]Department of Biological Sciences, Mississippi State University, Mississippi State, MS 39762, USA
*Author for correspondence: qianglv1982@126.com (Q.L.), wangleibailu@163.com (L.W.), liling@biology.msstate.edu (L.L.), yhe@cnu.edu.cn (Y.H.)
†These authors contributed equally to this work.
The authors responsible for the distribution of materials integral to the findings presented in this article in accordance with the policy described in the Instructions for Authors (https://academic.oup.com/plphys/pages/General-Instructions) are: Qiang Lv, Lei Wang, Ling Li, and Yikun He.
‡Present address: College of Life Sciences, Shihezi University, Shihezi 832003, China.

Abstract

Drought stress poses a substantial challenge to plant growth and agricultural productivity worldwide. Upon water depletion, plants activate an abscisic acid (ABA) signaling pathway, leading to stomatal closure to reduce water loss. The MYB family of transcription factors plays diverse roles in growth, development, stress responses, and biosynthesis, yet their involvement in stomatal regulation remains unclear. Here, we demonstrate that ABA significantly upregulates the expression of *MYB41*, *MYB74*, and *MYB102*, with MYB41 serving as a key regulator that induces the expression of both *MYB74* and *MYB102*. Through luciferase assays, chromatin immunoprecipitation (ChIP) assays, and electrophoretic mobility shift assays (EMSA), we reveal that MYB41 engages in positive feedback regulation by binding to its own promoter, thus amplifying its transcription in Arabidopsis (*Arabidopsis thaliana*). Furthermore, our investigation showed that MYB41 recruits BRAHMA (BRM), the core ATPase subunit of the SWI/SNF complex, to the *MYB41* promoter, facilitating the binding of HISTONE DEACETYLASE 6 (HDA6). This recruitment triggers epigenetic modifications, resulting in reduced *MYB41* expression characterized by elevated H3K27me3 levels and concurrent decreases in H3ac, H3K27ac, and H3K14ac levels in wild-type plants compared to *brm* knockout mutant plants. Our genetic and molecular analyses show that ABA mediates autoregulation of the MYB41-BRM module, which intricately modulates stomatal movement in *A. thaliana*. This discovery sheds light on a drought response mechanism with the potential to greatly enhance agricultural productivity.

Introduction

Plants, being sessile organisms, are susceptible to various stresses, including both abiotic and biotic factors (Cramer et al. 2011). Among these stressors, drought stands out as a significant abiotic challenge, threatening plant growth and agricultural productivity (Zhu 2016). A key regulator in the response to drought is abscisic acid (ABA), a pivotal phytohormone that significantly increases under drought conditions. ABA initiates diverse plant responses, including stomatal closure and alterations in gene expression, thereby enhancing the plant's ability to cope with stress (Kim et al. 2010; Zhu 2016; Vishwakarma et al. 2017; Lim et al. 2022). Signal molecules such as nitric oxide (NO) and reactive oxygen species (ROS) have been identified as integral components of the ABA-mediated signaling cascade governing stomatal closure. ABA treatment enhances NO synthesis in guard cells, where NO plays a critical role in ABA-induced stomatal closure (Garcia-Mata and Lamattina 2003; Yan et al. 2007; Neill et al. 2008, Gan et al. 2015; Majeed et al. 2020; Shen et al. 2021).

One prominent player in plants is BRAHMA (BRM), an ATPase subunit of the Switch/Sucrose Non-Fermentable (SWI/SNF) complex, analogous to the putatively paralogous found in yeast and animal SWI/SNF ATPases (Thouly et al. 2020). The SWI/SNF complex regulates the transcriptional expression of specific genes, thereby influencing growth, development, and stress tolerance in plants (Wagner and Meyerowitz 2002; Farrona et al. 2004; Hurtado et al. 2006; Archacki et al. 2009; Li et al. 2015; Cho et al. 2016; Sarnowska et al. 2016; Xu et al. 2016). Interestingly, BRM can antagonize the ABA signaling pathway under normal conditions, yet the *brm* mutant exhibits enhanced drought tolerance (Han et al. 2012). Further research has revealed that core components of the ABA signaling network interact with BRM. Dephosphorylation of BRM by protein phosphatase 2 catalytic subunit alpha (PP2CA) leads to its inactivation, while BRM phosphorylation by SNF1-related protein kinase 2 (SnRK2) restores its activity, allowing it to counteract plant responses to ABA treatment (Peirats-Llobet et al. 2016).

Autoregulation, the ability of genes to influence their own expression, impacts various aspects, such as stabilizing transposons in genomes (Bateman 1998; Carrier and Keasling 1999; Claeys Bouuaert et al. 2013; Wang and He 2023), affecting cell behavior (Kang et al. 2014), cell phenotype (Barros et al. 2011) and cancer development (Chen et al. 2016). In the realm of plants, the flowering regulator SUPPRESSOR OF OVEREXPRESSION OF CONSTANS 1 (SOC1) has been implicated in autoregulation,

Received August 30, 2023. Accepted June 1, 2024.

potentially moderating its flowering pace in response to environmental cues in Arabidopsis (*Arabidopsis thaliana*) (Richter et al. 2019). Autoregulation of the *MYB10* gene led to increased transcript levels and elevated anthocyanin accumulation in apples (Espley et al. 2009). AGAMOUS-Like 15 (AGL15), a regulatory factor with a MADS (MCM1, AGAMOUS, DEFICIENS, and SRF, serum response factor) domain in *A. thaliana*, influenced embryogenesis via autoregulation (Zhu and Perry 2005). Similarly, ARABIDOPSIS THALIANA HOMEOBOX PROTEIN 2 (ATHB-2) demonstrated a negative autoregulatory loop that mediated light signals during morphogenesis in *A. thaliana* (Ohgishi et al. 2001).

The V-myb avian myeloblastosis viral oncogene homolog (MYB) protein constitutes one of the largest transcription factor families in plants. In *A. thaliana*, the R2R3 type MYB transcription factor gene family comprises 125 members that play a role in regulating diverse processes such as biosynthesis, development, and abiotic stress response (Dubos et al. 2010; Gan et al. 2015; Daneva et al. 2016; Ma and Constabel 2019). MYB41 is influenced by transcriptional regulation in response to salt, drying and low temperature, helping to balance endogenous ABA levels (Cominelli et al. 2008; Lippold et al. 2009). Under salt stress in *A. thaliana*, MYB41 can also be activated by MPK6 (Mitogen-activated protein kinase 6)-mediated phosphorylation (Hoang et al. 2012). Moreover, MYB41 triggers suberin synthesis and deposition in the cell wall, enhancing drought resistance in both *A. thaliana* and *Nicotiana benthamiana* (Kosma et al. 2014). Notably, the *myb41 myb53 myb92 myb93* quadruple mutant plants show reduced stress-induced corkification of roots in *A. thaliana* (Shukla et al. 2021), offering insights into the molecular mechanisms governing root development and stress adaptation (Xu et al. 2022). Phylogenetic analysis reveals that *AtMYB41* (At4g28110), along with *AtMYB74* (At4g05100) and *AtMYB102* (At4g21440), belongs to subgroup 11 of the R2R3-MYB transcription factor family of Arabidopsis (Stracke et al. 2001; Jiang and Rao 2020). Recent research has demonstrated that *MYB41*, *MYB74*, *MYB9* (At5g16770), and *MYB39* (At4g17785) form a transcriptional cascade in response to ABA treatments (Xu et al. 2022). Interestingly, within this subgroup, there are no studies exploring the role of stomatal regulation in drought.

In this investigation, we evaluated the transcriptional responses of six members from subgroup 11 and subgroup 10, including *AtMYB41*, *AtMYB74*, *AtMYB102*, *AtMYB9*, *AtMYB39*, and *AtMYB107* (At3g02940), upon exposure to ABA treatment. Among these, MYB41, MYB74, and MYB102 emerged as key participants in ABA-mediated stomatal regulation. To elucidate the mechanism by which these MYBs influence water balance through stomatal control, we integrated genetic findings with biochemical and molecular analyses. Our investigation reveals that the ABA-mediated autoregulation of MYB41 is inhibited by BRM, which is recruited by MYB41 to its own transcriptional region. This interaction triggers epigenetic modification on histones within the binding sites, suggesting a precise regulatory mechanism for controlling stomatal movement in *A. thaliana*.

Results

MYB41, MYB74, and MYB102 play a key role in regulating ABA-mediated stomatal movement

To explore the potential involvement of six members of the MYB transcription factor family (*MYB41*, *MYB74*, *MYB9*, *MYB39*, *MYB102*, and *MYB107*) in ABA signaling, we tested their transcriptional responses under ABA treatments. Notably, *MYB41* exhibited a substantial increase in expression at 1 h, reaching over a 100-fold increase at 3 h, while *MYB74* and *MYB102* showed increases of more than 30 and 50 times, respectively, at 3 h of ABA treatment. However, the expression levels of *MYB9*, *MYB39*, and *MYB107* remained relatively unchanged (Fig. 1A). These results indicated that *MYB41*, *MYB74*, and *MYB102* were responsive to ABA treatment and warranted further investigation in this study.

To gain insights into the spatiotemporal expression pattern of *MYB41* under ABA treatment, we utilized the *pMYB41:GUS* reporter system. Our observations revealed predominant localization of MYB41 in leaf veins and stomata (Fig. 1B; Supplementary Fig. S1). The promoter activity of *MYB41* was enhanced in stomata under ABA treatment, implying its potential role in regulating ABA-mediated stomatal movement.

Subsequently, to assess the genetic role of MYB41 in stomatal regulation, we generated CRISPR alleles of *MYB41:myb41* by introducing a one-base pair addition at the beginning of the first exon of the *MYB41* gene (Supplementary Fig. S2A). This was done due to the unavailability of a *myb41* T-DNA knockout mutant from the Arabidopsis Biological Resource Center (https://abrc.osu.edu). Upon comparing stomatal responses to ABA treatment between *myb41* mutants and wild-type (WT) plants, we calculated the ratio of width to length of the stomatal aperture. We observed no significant difference in stomatal aperture under normal conditions. However, intriguingly, the *myb41* mutants exhibited significantly wider stomatal apertures compared to WT plants under ABA treatment (Fig. 1, C and D). This indicates a positive role of MYB41 in ABA-induced stomatal closure.

To further elucidate the roles of MYB74 and MYB102 in regulating stomatal aperture, we obtained homozygous T-DNA insertion mutants for *myb74* and *myb102*. Subsequently, we examined their stomatal apertures under ABA treatment conditions. Intriguingly, both *myb74* and *myb102* mutants exhibited remarkably similar phenotypes to *myb41* when compared to WT (Supplementary Fig. S3, A and B).

These results imply functional redundancy among *MYB41*, *MYB74*, and *MYB102* in response to ABA. To uncover other potentially active MYBs in *myb41* mutants, we assessed the transcript levels of various MYB candidates in both WT and *myb41* mutant backgrounds. Under ABA treatment, we observed a slightly lower *MYB74* transcript level in the *myb41* mutant compared to WT plants, while the *MYB102* transcript level was slightly elevated in the *myb41* mutant (Fig. 1, E and F).

Our observations suggest that a group of MYB transcription factors, rather than a single MYB, likely collectively govern stomatal closure. To test this hypothesis, we harnessed CRISPR technology to introduce frameshift mutations that disrupt the function of *MYB41* and *MYB102* in *myb74* and Col-0 backgrounds (Supplementary Figs. S2 and S3, A and B). Subsequently, we assessed stomatal aperture in resulting double mutant *myb41 myb102* (*doub-myb*), *myb41 myb74*, and triple mutant *myb41 myb74 myb102* (*trip-myb*) plants.

Under normal growth conditions, the stomatal aperture of *myb41* and *doub-myb* resembled that of WT. However, *trip-myb* exhibited slightly more open stomata than WT. Following ABA treatments, while WT stomata exhibited significant closure, mutant plants displayed impaired stomatal aperture closure, particularly evident in *trip-myb* plants where stomata showed inadequate response to ABA treatments (Fig. 1, G and H; Supplementary Fig. S3, C to F).

Stomatal aperture closure is crucial for preventing water loss in plants. Therefore, we assessed the water-loss rates from detached leaves of WT, *myb41*, *myb74*, *myb102*, *doub-myb*, and *trip-*

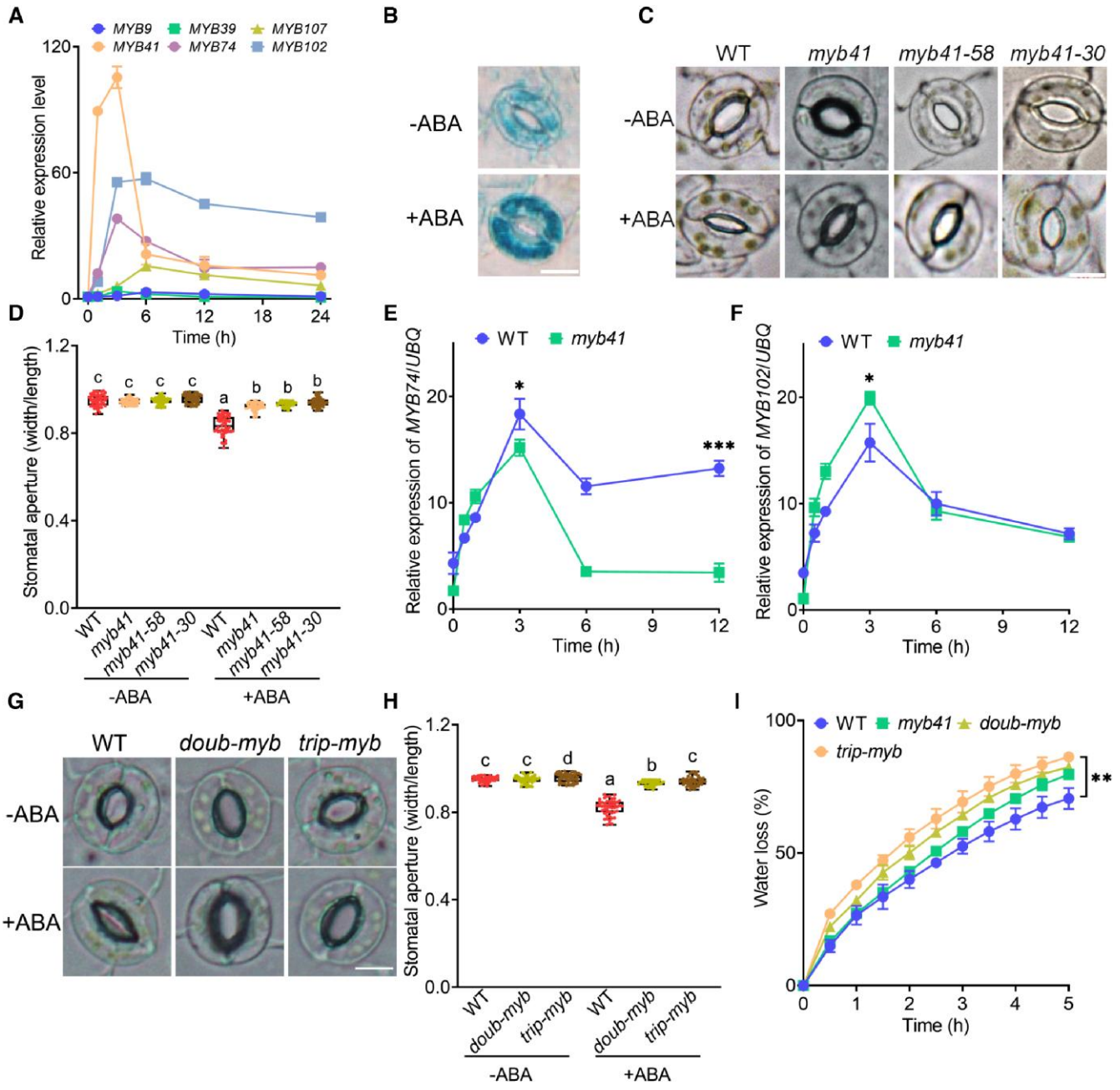

Figure 1. *MYB41* rapidly responds to ABA to promote stomatal closure. **A)** Relative expression levels of candidate *MYB* genes in wild type (WT). Seven-day-old seedlings were treated with either 0 μM abscisic acid (ABA [Control]) or 10 μM ABA for 1, 3, 6, 12, and 24 h, followed by total RNA extraction. Data represent means ± SD of 3 independent experiments. Error bars are overlaid by symbols when not visible. **B)** At*MYB41* expression patterns observed in 7-d-old At*MYB41promoter:GUS* transgenic seedlings grown on 1/2 MS medium and transferred to fresh medium without ABA (top), or with 10 μM ABA for 3 h (bottom). Scale bar, 10 μm. **C** and **D**) Abaxial epidermal strips of WT, *myb41*, *myb41-58*, and *myb41-30* plants were incubated in MES buffer with or without 10 μM ABA for 0.5 h. In (C), representative images of guard cells captured at 20× magnification. Scale bar, 10 μm. In (D), stomatal apertures were measured in epidermal strips, presenting the ratio of width to length of stomata. Data are presented using box and whiskers plots, where the whiskers denote the minimum and maximum values, and the box represents the second quartile, median and third quartile ($n = 60$). Different letters denote significant differences according to one-way ANOVA with the Tukey test ($P < 0.05$). **E** and **F**) Relative expression levels of the *MYBY74* and *MYB102* in WT and *myb41*. Seven-day-old seedlings were treated with 0 μM ABA (Control) or 10 μM ABA for 1, 3, 6, and 12 h, followed by total RNA extraction. Data represent means ± SD of 3 independent experiments. Error bars are overlaid by symbols when not visible. Asterisks indicate significant differences (*$P < 0.05$, ***$P < 0.001$; Student's *t*-test). **G** and **H**) Abaxial epidermal strips of WT, *myb41 myb102* (*doub-myb*), and *myb41 myb74 myb102* (*trip-myb*) plants were incubated in MES buffer with or without 10 μM ABA for 0.5 h. In (**G**), representative images of guard cells captured at 20× magnification. Scale bar, 10 μm. In (**H**), stomatal apertures were measured in epidermal strips, presenting the ratio of width to length of stomata. Data are presented using box and whiskers plots, where the whiskers denote the minimum and maximum values, and the box represents the second quartile, median and third quartile ($n = 60$). Different letters indicate significant differences according to one-way ANOVA with Tukey test ($P < 0.05$). **I)** Water loss of detached leaves of WT, *myb41*, *doub-myb*, and *trip-myb* plants. Values represent means ± SD of 3 independent experiments. Error bars are overlaid by symbols when not visible. Asterisks indicate significant differences (**$P < 0.01$; Student's *t*-test).

myb plants under constant temperature and light conditions. Remarkably, *myb41*, *myb74*, and *myb102* single mutants displayed higher water-loss rates compared to WT, without significant changes in stomatal density (Fig. 1I; Supplementary Fig. S4A). The *trip-myb* mutant exhibited the highest water-loss rate, followed by *doub-myb* and *myb41*, while WT had the lowest water-loss rate (Fig. 1I; Supplementary Fig. S4, B and C), and none of them displayed altered stomatal density (Supplementary Fig. S5, A to D). The observation of the highest water-loss rate in *trip-myb* is consistent with its more open stomatal aperture compared to WT.

Additionally, we evaluated the drought resistance of WT, *myb41*, *doub-myb*, and *trip-myb* plants in soil. After subjecting the plants to 21 d of drought followed by 7 d of rehydration, WT displayed a survival rate of approximately 80%, whereas *trip-myb* mutant exhibited a significantly lower survival rate of around 50%. These findings underscore the heightened drought sensitivity of *trip-myb* mutant (Fig. 2, A and B).

The protein kinase OPEN STOMATA 1 (OST1) is known to facilitate the reduction of stomatal apertures, playing a pivotal role in ABA-induced stomatal closure (Mustilli et al. 2002). To explore whether these signaling components are integral to MYB41-triggered stomatal closure, we utilized the OST1 T-DNA insertion allele *ost1-3* (salk_008068) (Waadt et al. 2015) and generated a double mutant, *myb41 ost1-3*. Our investigation revealed that MYB41-induced stomatal closure was compromised in *ost1-3* mutants (Supplementary Fig. S6). This outcome suggests that the guard cell signaling mediated by MYB41 operates in an ABA-dependent manner, requiring OST1 for effective stomatal closure.

Controlling stomatal closure and NO biosynthesis: role of MYBs in ABA-mediated regulation

Numerous investigations have underscored the significance of NO in ABA-mediated stomatal closure during drought stress in plants (Gan et al. 2015; Majeed et al. 2020; Shen et al. 2021). To assess ABA-induced NO production in guard cells, we employed the NO-sensitive fluorescent probe DAF-FM-DA. Notably, under normal conditions, the levels of NO in *myb41*, *myb74*, *myb102*, *doub-myb*, and *trip-myb* mutants were marginally lower than those in WT. Conversely, upon ABA treatment, the mutant plants exhibited compromised NO accumulation in comparison to WT, leading to a significant reduction in fluorescence intensity (Fig. 2, C and D; Supplementary Fig. S7, A to F). Both the phenotypes of stomatal closure and NO accumulation exhibited an ABA-treated time-dependent manner (Supplementary Fig. S8). Given that the main pathways for NO production in plants are the NOS pathway and the NR pathway (Wilson et al. 2008), we proceeded to examine the transcript levels of key genes affecting the NR pathway, namely nitrate reductase 1 and nitrate reductase 2 (*NIA1* and *NIA2*), and genes influencing the NOS pathway, such as nitric oxide-associated 1 (*NOA1*), in the mutants (*myb41*, *doub-myb,* and *trip-myb*). The results revealed that there was repression in the transcript levels of all these 3 genes—*NIA1*, *NIA2*, and *NOA1*—in these mutants (Supplementary Fig. S9). This observation suggests that MYB transcription factors impede NO accumulation by influencing both the NOS and NR pathways. These findings underscore the pivotal role of MYBs in ABA-triggered NO synthesis for effective stomatal closure.

To elucidate the interplay involving MYB41 and other MYBs, we generated *pER8GW:MYB41* transgenic plants, wherein *MYB41* expression could be induced by estradiol application. Impressively, after 3 h of estradiol induction, *MYB41* expression exhibited a remarkable surge of over 80-fold (Fig. 2E). Concurrently, the expression levels of *MYB9*, *MYB74*, *MYB102*, and *MYB107* also experienced upregulation in the *pER8GW:MYB41* transgenics following the same induction period. This observation hints at a potential regulatory influence of MYB41 over these MYBs (Fig. 2E).

Furthermore, in-depth RT-qPCR analysis unveiled distinct responses to ABA treatment within *myb41*, *doub-myb*, *trip-myb*, and WT, with significantly reduced *MYB41* expression levels in the mutant variants (Fig. 2F). To explore the possibility of an autoregulatory mechanism governing *MYB41*, we conducted an investigation using F1 plants derived from a cross between *pER8GW:MYB41* and *pMYB41:GUS* plants. We evaluated the transcript levels of both *MYB41* and *GUS* under various conditions. Notably, relative *MYB41* expression levels were substantially induced upon estradiol treatment in these F1 plants. Intriguingly, the relative *GUS* expression levels also displayed a significant increase following estradiol treatment (Fig. 2G). This phenomenon implies that estradiol treatment promotes *MYB41* expression due to the presence of *pER8GW:MYB41* in F1 plants. Subsequently, the elevated *MYB41* levels may trigger the regulation of its own promoter, leading to the induction of *GUS* expression, as a result of the presence of *pMYB41:GUS* in these F1 plants. This suggests a plausible mechanism of self-regulation. Collectively, these compelling findings underscore the pivotal roles played by the MYB41, MYB74, and MYB102 transcription factors in controlling stomatal closure and NO biosynthesis as part of ABA-induced responses to drought stress. Additionally, these findings suggest the existence of an autoregulatory mechanism within *MYB41*'s regulatory network.

In addition, we investigated the ABA response phenotypes in seed germination and seedling growth of WT, *myb41*, *doub-myb*, and *trip-myb*. Under normal conditions, there were no discernible differences in the germination rates and seedling growth among WT, *myb41*, *doub-myb,* and *trip-myb*. However, upon treatment with 0.5 μM ABA and 1 μM ABA, *trip-myb* exhibited higher germination rates and root growth, exhibiting insensitivity to ABA treatment compared to WT (Supplementary Fig. S10).

MYB41 orchestrates self-regulation through direct interaction with its promoter

To elucidate the underlying self-regulatory mechanism of MYB41, we used a *trip-myb* protoplast transient luciferase assay system. In this approach, various truncated DNA fragments of the *MYB41* promoter sequence were coupled with the *LUC* reporter gene, while the *MYB41* coding sequence (CDS) was overexpressed as the effector (Fig. 3A). The results of this analysis unveiled a significant elevation in promoter activity in the presence of *MYB41* CDS (Fig. 3B), strongly suggesting the existence of an autoregulation within MYB41. Intriguingly, the promoter activity exhibited a substantial enhancement when encompassing the 2 k to 1.5 k upstream region, suggesting the potential presence of pivotal regulatory motifs within this segment (Fig. 3B). Utilizing bioinformatics tools, we predicted the *MYB41* promoter region (Supplementary Table S1) and identified a putative enhancer binding site motif labeled as "ATTACT" (http://www.enhanceratlas.org/browseenhancer.php?enhancer=DM002-14830), located within the upstream 2 k to 1.5 k region (Fig. 3C). Notably, mutation of this identified motif led to a significant reduction in promoter activity (Fig. 3D), underscoring the significance of this motif in governing *MYB41* promoter activity.

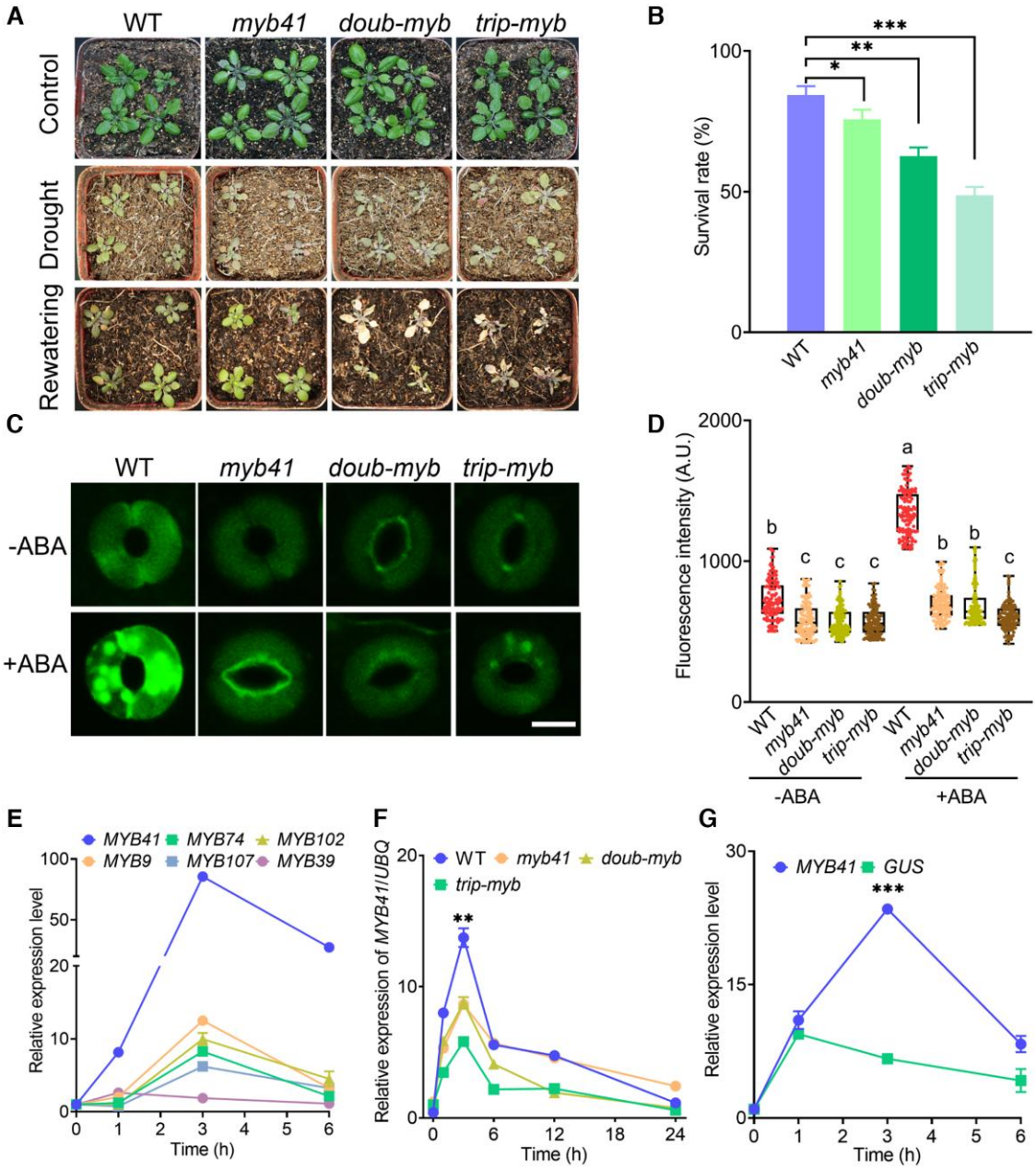

Figure 2. MYB41 promotes drought tolerance correlated with nitric oxide content. **A)** Plant images (left) and **B**) survival rates (right) of 14-d-old soil-grown plants without watering for 14 d. Plants of distinct genotypes were randomly placed in the tray, as indicated in the schematic diagram. Images were captured at 28 d (post-drought stress), and 33 d (post-rewatering), with the survival rate assessed 7 d after rehydration. Data in (B) represent means ± SD ($n = 36$ plants per group; from 3 independent experiments). Asterisks indicate significant differences (*$P < 0.05$, **$P < 0.01$, ***$P < 0.001$; Student's *t*-test). **C** and **D**) Epidermal strips of wild-type (WT), *myb41*, *doub-myb*, and *trip-myb* plants were incubated in MES buffer alone (Control) or with 10 μM abscisic acid (ABA) for 0.5 h. Representative images (C) and fluorescence intensities (D) of guard cells preloaded with 10 mM fluorescent probe DAF-FM-DA (for nitric oxide (NO) detection). For (C), scale bar = 10 μm. For (D), data are presented using box and whiskers plots, where the whiskers denote the minimum and maximum values, and the box represents the second quartile, median, and third quartile ($n = 120$). Different letters indicate significant differences according to one-way ANOVA with the Tukey test ($P < 0.05$). **E)** Relative expression levels of candidate *MYB* genes in *pER8GW:MYB41* plants treated with 5 μM estradiol for 1, 3, and 6 h, followed by total RNA extraction. Data represent means ± SD of 3 independent experiments. Error bars are overlaid by symbols when not visible. **F)** Relative expression levels of *MYB41* in WT, *myb41*, *doub-myb*, and *trip-myb* plants. Seven-day-old seedlings were treated with 0 μM ABA (Control) or 10 μM ABA for 1, 3, 6, 12, and 24 h, followed by total RNA extraction. Data represent means ± SD of 3 independent experiments. Error bars are overlaid by symbols when not visible. Student's *t*-test was used to determine statistical significance of difference from *trip-myb* (**$P < 0.01$). **G)** Relative expression levels of the *MYB41* and *GUS* genes in the F1 plants from the cross of *pER8GW:MYB41* and *pMYB41:GUS* plants, when treated with 5 μM estradiol for 1, 3, and 6 h, followed by total RNA extraction. Data represent means ± SD of 3 independent experiments. Error bars are overlaid by symbols when not visible. Asterisks indicate significant differences (***$P < 0.001$; Student's *t*-test).

Subsequently, we generated stable transgenic Arabidopsis plants by fusing the upstream 2 k, 1.5 k, and mutated binding site 2 k (2 k-mut) promoters with GUS and introducing them into both WT and triple mutant backgrounds. Qualitative assessment of GUS expression depicted robust staining for the 2 k fragment in WT, indicating the highest activity (Fig. 3, E and F). Conversely, reduced activity was discerned in the 1.5 k and 2 k-mut fragments, suggesting the critical role of this site in MYB41's autoregulation (Fig. 3, E and F). Moreover, upon fusing the "2 k" promoter of *MYB41* with a GUS gene sequence, a conspicuous reduction in

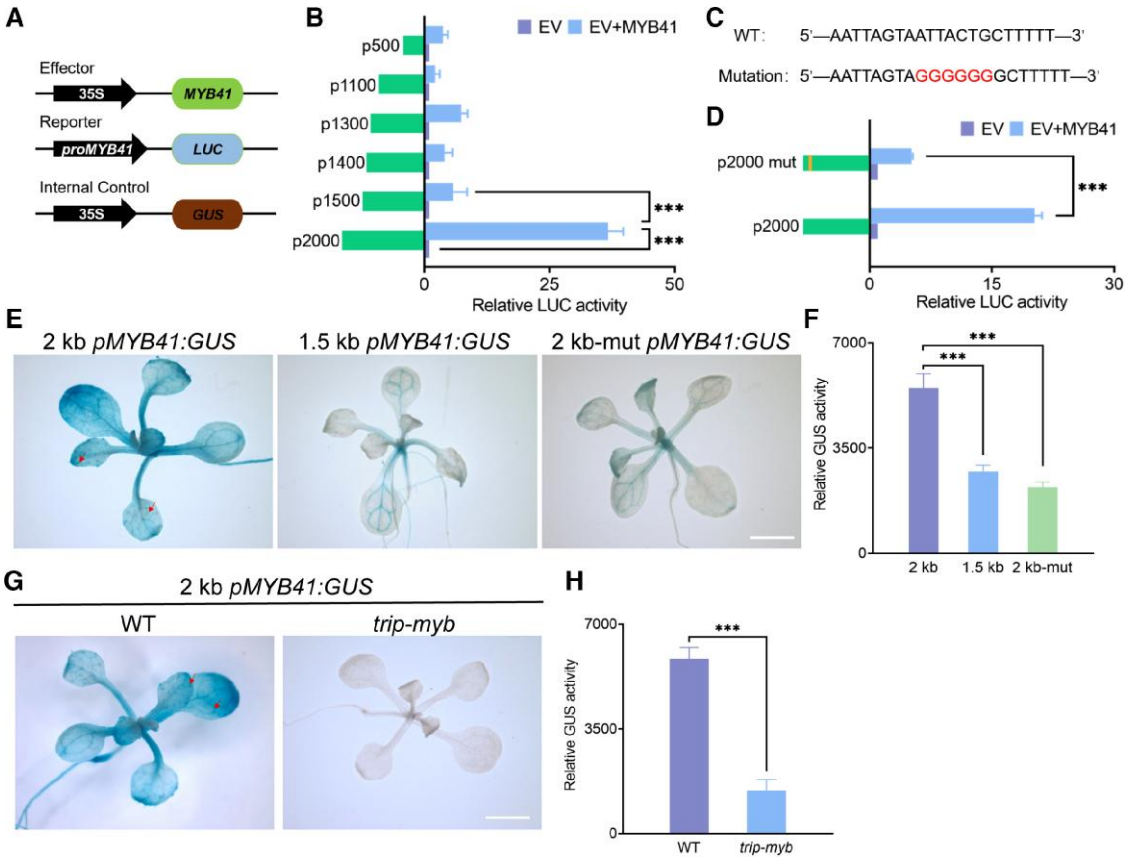

Figure 3. <>MYB41's autoregulatory control of its own promoter activity. **A)** Schematic representation of reporter and effector constructs used for the LUC assay. Co-infiltration of reporter, effector and control into *A. thaliana* leaf protoplasts enabled assessment of LUC activity regulation. **B)** Protoplasts were co-transformed with the *pMYB41:LUC* reporter (fused with p500, p1100, p1300, p1400, p1500, p2000) and a *MYB41*-overexpressing effector (*35S:MYB41*). The *35S:GUS* construct served as an internal effector control. **C)** Schematic depiction of the mutation site within the *MYB41* promoter 2-kb region. **D)** Protoplasts were co-transformed with the *pMYB41:LUC* reporter (fused with p2000 and p2000 mutation as shown in (C)) and a *MYB41*-overexpressing effector (*35S:MYB41*). The *35S:GUS* construct served as an internal effector control. In (B and D), relative reporter activity was normalized using the LUC/GUS ratio, with the ratio arbitrarily set to 1. Data represent means ± SD of 3 biological replicates. Asterisks indicate significant differences (***$P < 0.001$; Student's *t*-test). **E)** Representative GUS staining outcomes of *pMYB41:GUS* transgenic plants in the wild-type (WT) background. Seedlings were germinated and grown on 1/2 MS medium for 14 d, followed by a 3-h treatment with 10 μM abscisic acid (ABA) ($n = 10$ transgenic plants). Scale bar = 1 mm. **F)** Quantitative 4-methylumbelliferyl glucuronide (MUG) assays performed on transgenic plants, as indicated in the left panel. Data are shown as means ± SD for 3 biological replicates. Asterisks indicate significant differences (***$P < 0.001$; Student's *t*-test). G and H) GUS staining and MUG assays of transgenic seedlings harboring the 2-kb *MYB41* promoter-*GUS* construct in both WT and *trip-myb* backgrounds. Seedlings were germinated and cultivated on 1/2 MS medium for 14 d, followed by a 3-h treatment with 10 μM ABA ($n = 10$ transgenic plants). Scale bar = 1 mm. Data in (H) are presented as means ± SD for 3 biological replicates. Asterisks indicate significant differences (***$P < 0.001$; Student's *t*-test). The red arrows indicated the expression in guard cells in (E) and (G).

MYB41 promoter activity was evident in *trip-myb* compared to WT, indicating the diminished expression of *MYB41* due to loss of function in MYB41, MYB74, and MYB102 (Fig. 3, G and H). This finding hints at the potential regulatory roles of MYB41, MYB74, and MYB102 in modulating *MYB41* promoter activity.

Furthermore, we carried out chromatin immunoprecipitation (ChIP)-qPCR experiments to ascertain the direct binding of MYB41 to its own promoter. Five fragments containing potential binding motifs were used for analysis (Fig. 4A). The findings showcased significant enrichment of *pMYB41-1* within the 1.5 to 2 k upstream region containing the motif "ATTACT" referred to in Fig. 3C, not the other 4 fragments, affirming the direct interaction of MYB41 with this specific region to foster self-expression (Fig. 4, A and B). Additionally, an electrophoretic mobility shift (EMSA) assay demonstrated that the recombinant GST-MYB41 protein directly engaged with the *pMYB41-1* promoter fragment, leading to a shift in mobility, unlike GST alone. Remarkably, elevated GST-MYB41 concentrations resulted in a more pronounced mobility shift (Fig. 4C).

BRM interacts with MYB41

Unraveling the regulatory intricacies of MYB41, we embarked on a mission to screen, identify, and scrutinize the functions of its interacting proteins. Yeast two-hybrid technology, as demonstrated by Efroni et al. (2013), unveiled a potential interaction between MYB41 and BRM. BRM, a pivotal core ATPase of the SWI/SNF complex, governs histone modification levels in target genes, thereby influencing gene expression. Given BRM's role in ABA signal transduction, we hypothesized its involvement in regulating ABA-triggered stomatal closure and its association with NO production regulation. We initiated the exploration by ascertaining the direct protein-protein interaction between BRM and MYB41. The BRM CDS sequence was partitioned into N, M, and C segments based on structural attributes and previous studies (Peirats-Llobet et al. 2016). Correspondingly, the MYB41 protein was dissected into N- and C-terminal domains, considering its DNA-binding and activation domains (Fig. 5A). These fragments of MYB41 and BRM CDS sequences were fused to the pGADT7 (AD) and pGBKT7 (BD) vectors, respectively, and

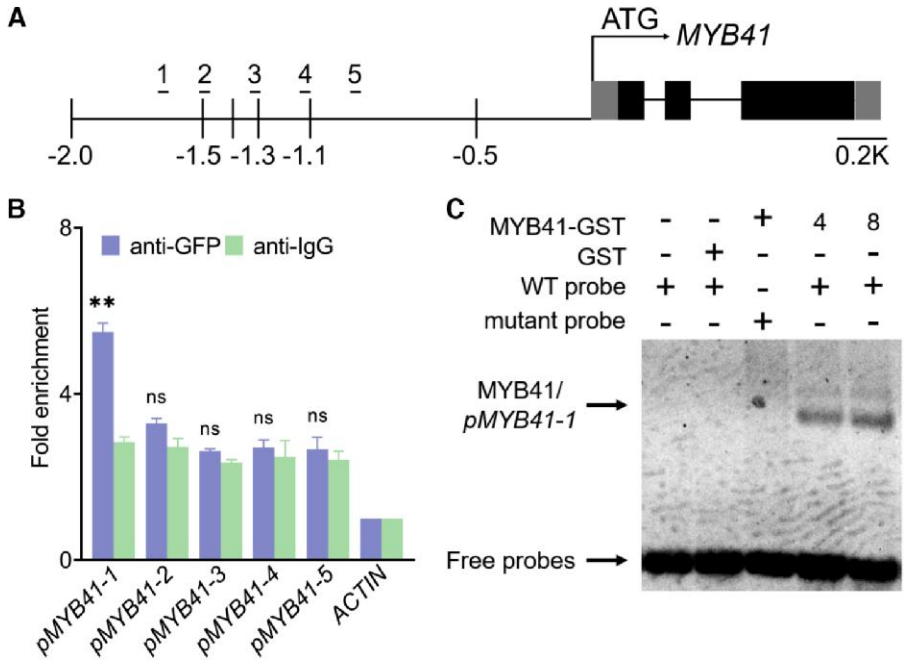

Figure 4. MYB41 directly binds to *pMYB41*. **A)** Schematic diagram of *MYB41* and its promoter genomic structure. Black boxes, exons; lines connecting the boxes, introns; and gray boxes, UTR. Five fragments containing each potential motif at *MYB41* promoter region were marked as "1," "2,""3," "4," and "5". **B)** ChIP experiments reveal MYB41 occupancy along *pMYB41* locus. Data are presented as a percentage of input. The anti-GFP antibody or anti-IgG was used to precipitate the protein–DNA complexes, while precipitation of *ACTIN* served as a negative control. Diagrams of the promoters and the regions ("1," "2," "3," "4," and "5") amplified by qPCR are illustrated in (A), Data represent means ± SD of 3 independent experiments. Error bars are overlaid by symbols when not visible. Statistical significance was determined using Student's *t*-test, (*$P < 0.05$, **$P < 0.01$, ***$P < 0.001$), while "ns" indicates no statistical significance. Specifically, *pMYB41-1* refers to the promoter region from −1,826 nt to −1,691 nt, *pMYB41-2* refers to the promoter region from −1,532 nt to −1,401 nt, *pMYB41-3* refers to the promoter region from −1,393 nt to −1,264 nt, *pMYB41-4* refers to the promoter region from −1,250 nt to −1,100 nt, and *pMYB41-5* refers to the promoter region from −1,087 nt to −929 nt. **C)** In vitro EMSA demonstrates MYB41 binding to *pMYB41-1*. Purified GST-tagged MYB41 protein was incubated with *pMYB41-1*, and resulting protein–DNA complexes were separated on native polyacrylamide gels. "-" and "+" denote "absence" and "presence", respectively. "4", "8" means 4 μg, 8 μg of MYB41-GST, respectively. Shifted bands and free DNA are indicated by black arrows. GST served as a negative control. The assay was replicated 3 times independently, yielding consistent outcomes.

co-transformed into yeast cells, followed by assessment of growth on selective media. Encouragingly, yeast cells harboring BRM-N (comprising the initial 711 amino acids and DVII domain) and MYB41 CDS fragments exhibited growth and developed a blue hue upon X-Gal staining, indicating direct protein-protein interaction. In contrast, neither the M and C segments nor negative controls devoid of exogenous fragments yielded positive outcomes (Fig. 5, B to D). Furthermore, we evaluated the interaction between the BRM-N segment and MYB41 N- and C-terminal domains using Bimolecular Fluorescent Complimentary (BiFC) experiments, revealing a distinct interaction pattern with MYB41 C-terminal region (Fig. 5E).

Subsequent verification of the physical interaction between BRM-N and MYB41 was constructed through pull-down assays. Prokaryotic expression vectors containing GST and MBP-His tags, namely pGEX-KG-MYB41 and pETMALc-H-BRM-DVII, were constructed. The target proteins were induced in *E. coli* and purified, followed by immunoprecipitation using GSH beads that bind to the GST tag. Western Blot (WB) analysis unveiled the formation of a band of equivalent size to GST-MYB41 protein upon co-incubation with MBP-His-DVII. In contrast, no such band was detected following MBP-His-DVII and GST co-incubation, firmly affirming the direct interaction between BRM-DVII and MYB41 (Fig. 5F).

BRM displays divergent regulatory dynamics from MYB41 in ABA-mediated stomatal movement and NO accumulation

To elucidate BRM's role in plant guard cell response to ABA signaling, functional partial deletion mutants of BRM, specifically *brm*-3 and *brm*-5, were obtained from ABRC (Tang et al. 2008; Zhang et al. 2017). Intriguingly, in contrast to *trip-myb*, both *brm*-3 and *brm*-5 mutants exhibited more closed stomatal apertures than those in WT, regardless of ABA treatment. This observation suggests BRM's involvement in suppressing ABA-induced stomatal closure, highlighting a contrasting regulatory pattern of BRM compared to MYB41 in the modulation of ABA-mediated stomatal movement (Fig. 6, A and B; Supplementary Fig. S11, A and B). Moreover, the NO content in *brm*-3 and *brm*-5 guard cells surpassed that in WT. However, under ABA treatment, while the NO content in WT guard cells significantly surged, *brm*-3 and *brm*-5 displayed nearly unaltered NO levels. This observation indicates *brm* plants' insensitivity to ABA and highlights BRM's role in inhibiting NO accumulation within guard cells (Fig. 6, C and D; Supplementary Fig. S11, C and D), consistent with our earlier findings. Notably, stomatal density remained unaffected in the *brm*-3 and *brm*-5 mutants (Supplementary Fig. S12A).

We further assessed the rate of water loss from detached leaves of WT, *brm*-3, and *brm*-5 mutant plants under consistent temperature and light conditions. In contrast to the *trip-myb* trend, intriguingly, the water-loss rate in the *brm*-3 and *brm*-5 mutants was notably lower than that in WT, regardless of stomatal density (Fig. 6G; Supplementary Fig. S12B). This finding indicates that BRM promotes water loss in Arabidopsis plants. Additionally, we examined the survival rates of WT, *brm*-3, and *brm*-5 mutant plants following drought treatment in soil. Interestingly, the *brm*-3 and *brm*-5 mutants exhibited enhanced drought tolerance compared to WT before rehydration, with a more pronounced difference at 7 d after rehydration. The survival rate for WT was

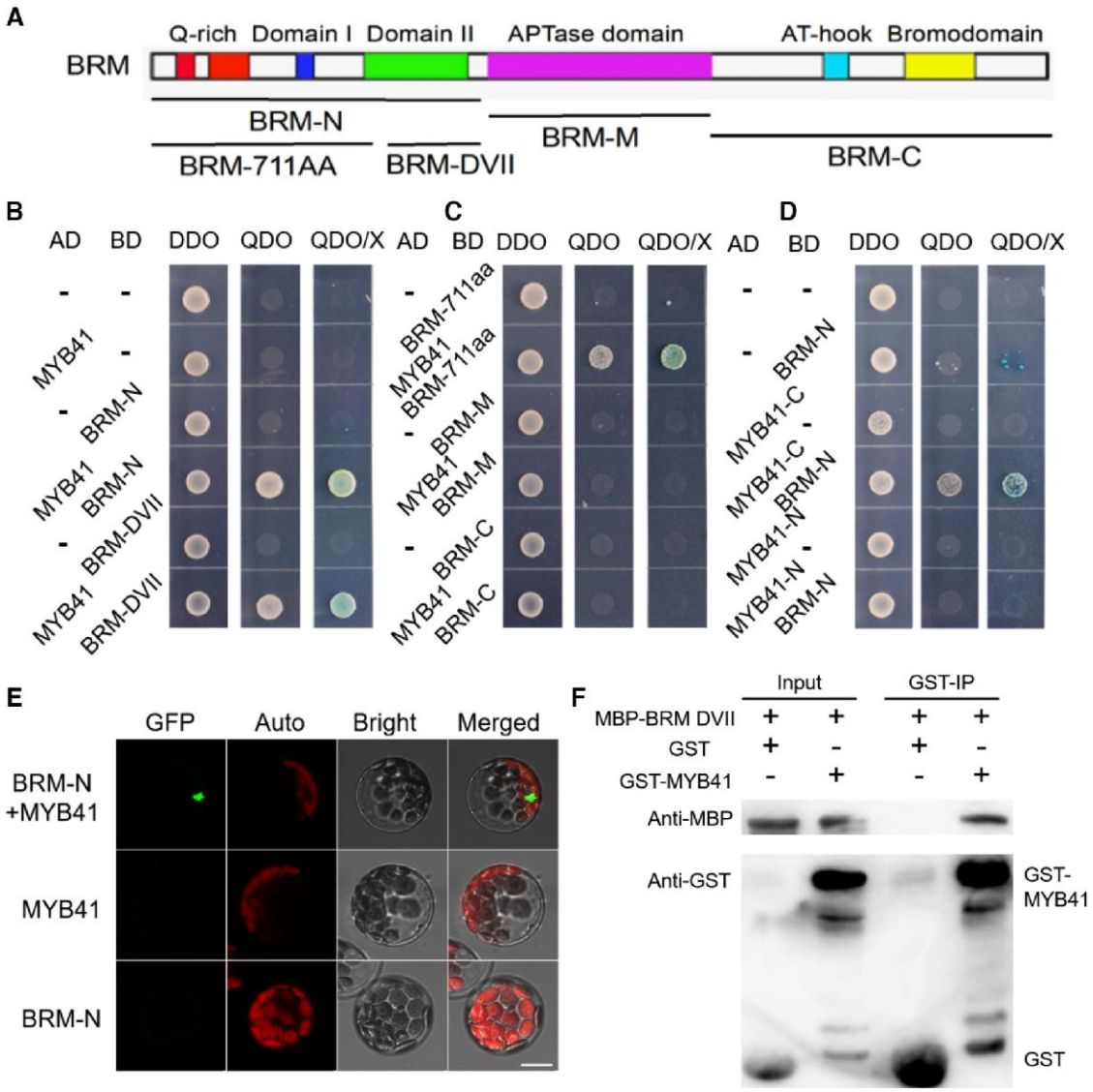

Figure 5. Interaction between BRM and MYB41. **A)** Diagram illustrating the full-length BRM and its various fragments used in the Y2H assay. The amino acid positions corresponding to these fragments are indicated. **B** to **D**) Y2H assay conducted to detect the interaction between MYB41 and BRM. The coding sequences of BRM-N, BRM-DVII, BRM-711aa, BRM-M, and BRM-C, as well as MYB41, MYB41-N, and MYB41-C, were inserted in-frame into BD or AD vectors. The appropriate combinations of constructs were co-transformed into yeast cells. The resulting transformants were plated on selective synthetic defined (SD) medium –Trp, –Leu and SD medium –Trp, –Leu, –His, –Ala to evaluate potential interactions. Yeast colonies were cultured on selective plates, and representative images from 3 independent yeast lines were captured after 4 d at 28 °C. An empty vector served as the negative control. **E)** BiFC assay demonstrating BRM-N interaction with MYB41 in Arabidopsis mesophyll protoplasts. Protoplasts were transfected with distinct combinations of expression vectors. Scale bar = 10 μm. **F)** In vitro pull-down assay. The N-terminal fragment of BRM (BRM-DVII) was fused with the MBP tag, and MYB41 was fused with GST. After co-incubation of the two proteins, complexes were precipitated with GST beads, and the presence of proteins was detected using anti-MBP and anti-GST antibodies.

merely 18%, whereas, for the *brm*-3 and *brm*-5 mutants, it stood at 92% and 73%, respectively, underscoring the heightened drought tolerance of these mutants (Fig. 6, E and F; Supplementary Fig. S12, C and D).

To elucidate the genetic relationship between BRM and MYBs, we generated a triple mutant (*myb41 myb74 brm*-5) and a quadruple mutant (*brm-3-trip-myb*, that is, *brm*-3 *myb41 myb74 myb102*) for analysis. The quadruple mutant *brm-3-trip-myb* and the *myb41 myb74 brm*-5 mutant exhibited phenotypes more similar to the *trip-myb* mutant and the *myb41 myb74* double mutant, respectively, than the single mutant *brm*-3 or *brm*-5, in terms of regulating ABA-mediated stomatal movement, NO accumulation, and drought tolerance (Fig. 6; Supplementary Fig. S13). These findings suggest that these MYBs likely function downstream of BRM.

Subsequent RT-qPCR analysis illuminated the shifts in *MYB41* expression levels across WT, *brm*-3, and *brm*-5 mutants. Remarkably, *MYB41* transcript levels were substantially elevated in the *brm*-3 and *brm*-5 mutants even without ABA treatment (Fig. 6H; Supplementary Fig. S12E). Under ABA treatment at different times (0, 1, 3, 6, 12, and 24 h), while *MYB41* expression levels in WT initially increased and then decreased, those in the *brm*-3 and *brm*-5 mutants exhibited significant changes. They rapidly peaked within 6 h and then swiftly declined, with the most marked difference observed at intermediate time intervals. Notably, *MYB41* expression levels in the *brm*-3 and *brm*-5 mutants were mostly higher than those in WT (except at 24 h), indicating BRM's sustained inhibitory effect on *MYB41* expression levels (Fig. 7A).

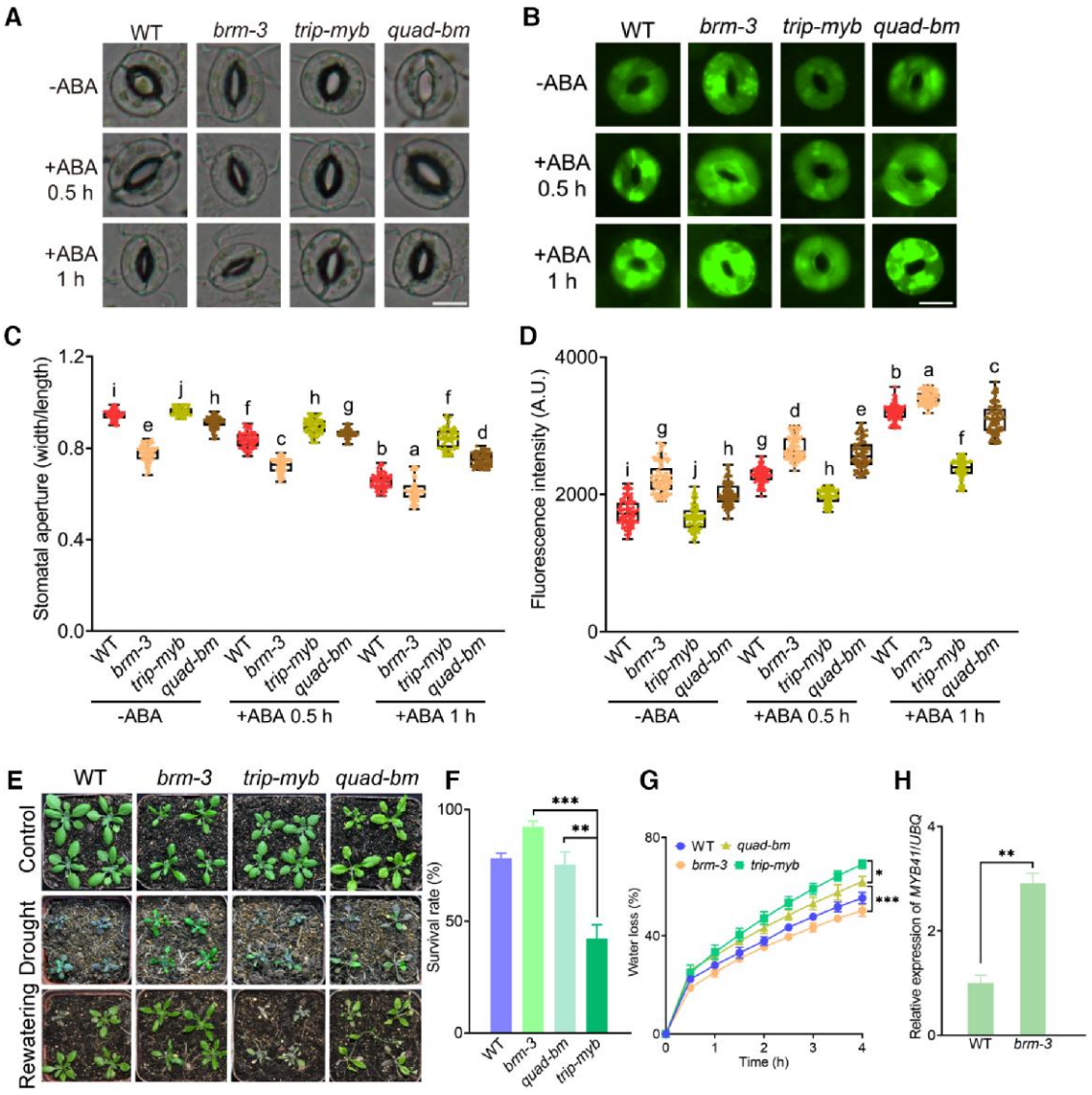

Figure 6. Contrasting effects of *brm* and *myb* on plant drought resistance. **A** and **B**) Abaxial epidermal strips of wild-type (WT), *brm-3*, *trip-myb* plants, and *brm-3-trip-myb* (*quad-bm*) plants were incubated in MES buffer with or without 10 μM abscisic acid (ABA) for 0.5 and 1 h. (A) Representative images of guard cells captured at 20× magnification. Scale bar, 10 μm. (B) Stomatal apertures were quantified in epidermal strips by determining the width-to-length ratio of stomata. Data are presented using box and whiskers plots, where the whiskers denote the minimum and maximum values, and the box represents the second quartile, median and third quartile ($n = 70$). Different letters indicate significant differences according to one-way ANOVA with the Tukey test ($P < 0.05$). **C** and **D**) Epidermal strips of WT, *brm-3*, *trip-myb*, and *brm-3-trip-myb* (*quad-bm*) plants were incubated in MES buffer alone (Control) or with 10 μM ABA for 0.5 and 1 h. Images (C) and fluorescence intensities (D) of guard cells preloaded with 10 mM of the fluorescent probe DAF-FM-DA (used for NO detection). For (C), scale bar = 10 μm. For (D), data are presented using box and whiskers plots, where the whiskers denote the minimum and maximum values, and the box represents the second quartile, median and third quartile ($n = 100$). Different letters indicate significant differences according to one-way ANOVA with the Tukey test ($P < 0.05$). **E** and **F**) Images (E) and survival rates (F) of 14-d-old plants grown in soil without watering for 14 d. Plants of different genotypes were randomly placed in a tray, as indicated in the schematic diagram. Images were captured at 28 d (post-drought stress), and 33 d (post-rewatering), with survival rate assessed 7 d after rehydration. Data in (F) represent means ± SD ($n = 36$ plants per group; data from 3 experiments). Asterisks indicate significant differences (**$P < 0.01$, ***$P < 0.001$; Student's *t*-test). **G)** Measurement of water loss from detached leaves of WT, *brm-3*, *trip-myb*, and *brm-3-trip-myb* (*quad-bm*) mutants. Values represent means ± SD of 3 independent experiments. Error bars are overlaid by symbols when not visible. Asterisks indicate significant differences (**$P < 0.01$; Student's *t*-test), while "ns" indicates no statistical significance. **H)** Relative expression levels of *MYB41* in WT and *brm-3* plants. Total RNA was extracted from 7-d-old seedlings. Data represent means ± SD of 3 independent experiments. Asterisks indicate significant differences (**$P < 0.01$; Student's *t*-test).

Furthermore, an investigation into the overexpression of *BRM* revealed intriguing findings. *BRM* overexpression (*BRM-OE*) displayed a contrasting pattern to the *brm* mutants and closely mirrored the behavior of the *trip-myb* mutant, particularly in stomatal closure and NO content (Supplementary Fig. S14, A to D).

Next, we examined the phenotypes of ABA responses in seed germination and seedling growth in WT, *brm-3*, *trip-myb*, and *brm-3-trip-myb* quadruple mutants, as well as in WT, *brm-5*, *myb74 myb102*, *myb74 myb102 brm-5* mutants. Unlike *myb74 myb102* and *trip-myb*, both *brm-3* and *brm-5* exhibited an ABA-hypersensitive phenotype in both seed germination and root growth compared to WT (Supplementary Figs. S15 and S16). Moreover, the *brm-3-trip-myb* quadruple mutant and *myb74 myb102 brm-5* exhibited a phenotype quite similar to *trip-myb* and *myb74 myb102*, respectively, with higher germination rates and a root growth insensitive phenotype compared to WT. It implies that the quadruple mutant, in which

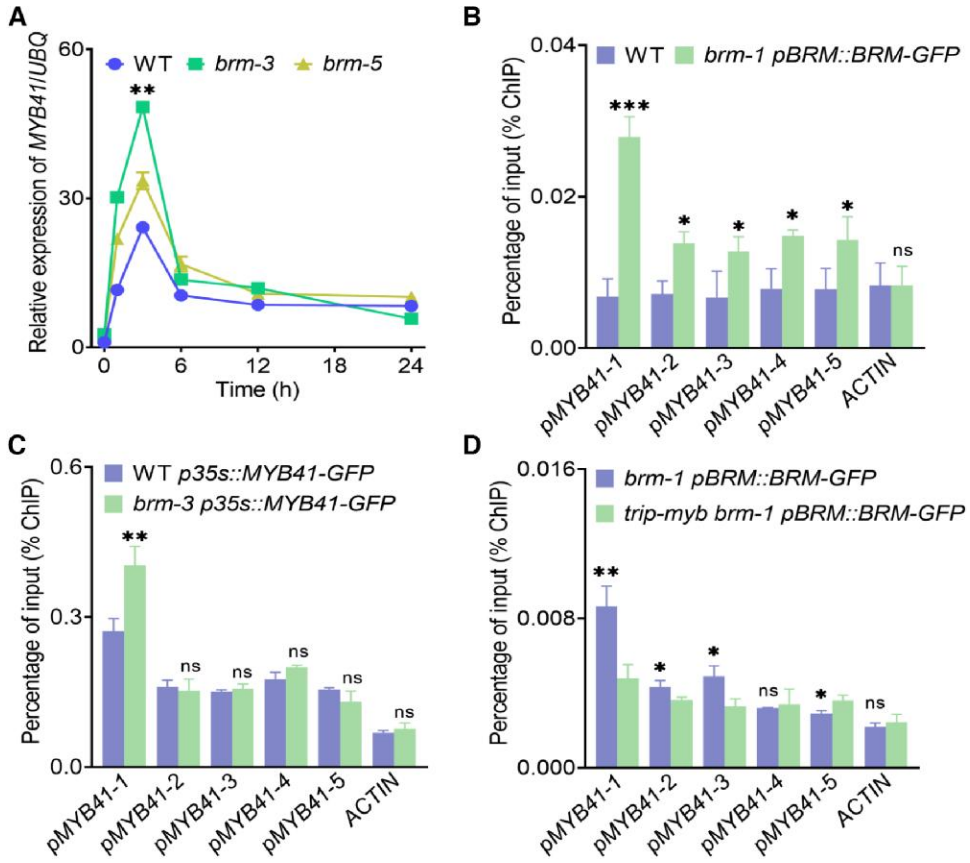

Figure 7. MYB41-mediated recruitment of BRM to inhibit *MYB41* expression. **A)** Relative expression levels of *MYB41* in wild-type (WT) and *brm*-3 plants. Seven-day-old seedlings were treated with 0 μM abscisic acid (ABA) (Control) or 10 μM ABA for 1, 3, 6, 12, and 24 h, followed by total RNA extraction. Data represent means ± SD of 3 independent experiments. Error bars are overlaid by symbols when not visible. Statistical significance was determined using Student's *t*-test, compared to WT (**$P < 0.01$). **B)** BRM occupancy analysis at selected genes by ChIP–qPCR, using anti-GFP antibody in WT and *brm-1 pBRM:BRM-GFP* plants. ChIP signals are depicted as a percentage of input. *ACTIN* was used as a negative control locus. Values represent means ± SD (3 biological replicates). **C)** MYB41 occupancy analysis at selected genes through ChIP–qPCR using anti-GFP antibody in WT *p35S:MYB41-GFP* and *brm-3 p35S:MYB41-GFP* plants. ChIP signals are presented as percentage of input. *ACTIN* served as a negative control locus. Values represent means ± SD (3 biological replicates). The experiments were performed twice with consistent results and one representative experiment is shown. **D)** BRM occupancy analysis at selected genes via ChIP–qPCR using anti-GFP antibody in *brm-1 pBRM:BRM-GFP* and *trip-myb brm-1 pBRM:BRM-GFP* plants. ChIP signals are shown as percentage of input. *ACTIN* was used as a negative control locus. Values represent means ± SD (3 biological replicates). The experiments were performed twice with consistent results, and one representative experiment is illustrated. In B to D), Statistical significance was determined using Student's *t*-test, compared to WT (*$P < 0.05$, **$P < 0.01$, ***$P < 0.001$), while "ns" indicates no statistical significance.

the mutation of *MYB41*, *MYB74*, and *MYB102* in the *brm*-3 mutant, or the mutation of *MYB74*, and *MYB102* in the *brm*-5 mutant, recovered the ABA-hypersensitive phenotype in seed germination and seedling root growth of *brm*-3 or *brm*-5, respectively (Supplementary Figs. S15 and S16). It indicates that these MYBs function downstream of BRM.

However, the phenotype of the *brm*-3-*trip-myb* quadruple mutant in stomatal movement and NO accumulation was observed to be intermediate between that of the *trip-myb* mutant and *brm*-3 (Fig. 6, A to G). This suggests that other MYBs might function redundantly with MYB41, MYB74, and MYB102. We examined the transcript level of 3 members in MYB Subgroup 10, *MYB9*, *MYB39*, and *MYB107*. We found that *MYB9* and *MYB39* were upregulated in *brm*-3 (Supplementary Fig. S17).

BRM collaborates with MYB41 to suppress MYB41's self-regulatory activity

In our quest to identify upstream regulators of the *MYB41* gene using Plant Regulomics, we uncovered BRM's potential to target the *MYB41* promoter (Supplementary Fig. S18, A and B). To further investigate the mechanism of BRM's interaction with the *MYB41* promoter, we utilized protoplasts from WT and *brm-1 pBRM:BRM-GFP*; WT *p35S:MYB41-GFP* and *brm-3 p35S:MYB41-GFP*; as well as *trip-myb brm-1 pBRM:BRM-GFP* and *brm-1 pBRM:BRM-GFP*. ChIP analysis was performed to determine the binding efficiency of MYB41 and BRM to the *MYB41* promoter. Strikingly, the enrichment efficiency of *MYB41* was notably higher in *brm-1 pBRM:BRM-GFP* compared to WT, particularly in *pMYB41-1* (Fig. 7B). Furthermore, the enrichment efficiency of *MYB41* was significantly elevated in *brm-3 p35S:MYB41-GFP* compared to WT *p35S:MYB41-GFP*, particularly in the "1" region, underscoring BRM's role in inhibiting MYB41's self-regulation (Fig. 7C). In addition, the enrichment efficiency of *pMYB41-1* was significantly higher in *brm-1 pBRM:BRM-GFP* compared to *trip-myb brm-1 pBRM:BRM-GFP*, suggesting that MYB can directly recruit BRM to bind to the *MYB41* promoter (Fig. 7D).

We proceeded with further experiments using both WT and *brm*-3 plant varieties to investigate whether BRM affects histone modification in the *MYB41* promoter region. Our ChIP assays revealed that BRM enhances the H3K27me3 levels within the *MYB41* promoter region in WT plants, contrasting with *brm*-3

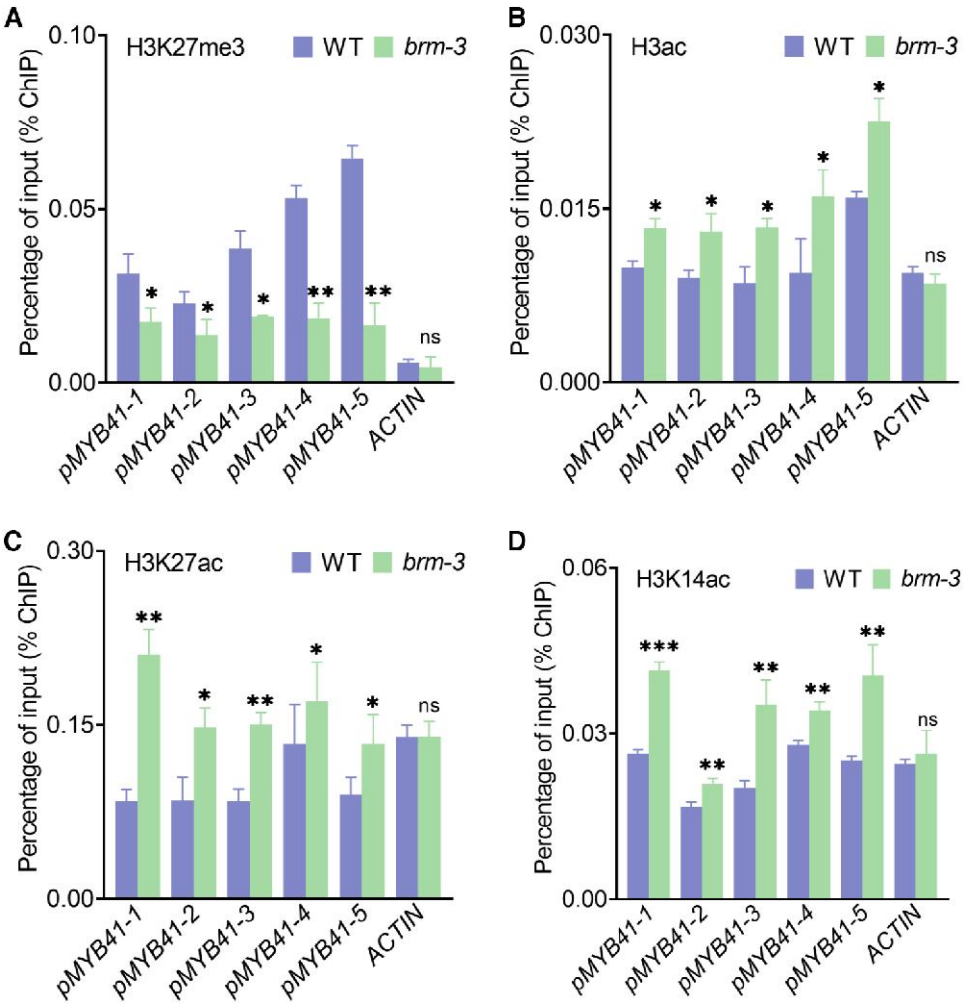

Figure 8. BRM modulates histone modifications at the *MYB41* promoter. **A** to **D**) ChIP–qPCR analysis of H3K27 methylation, H3, H3K14, and H3K27 acetylation levels at *MYB41* locus in wild-type (WT) and *brm-3* seedlings cultured on 1/2 MS medium for 14 d. ChIP signals are depicted as percentage of input. *ACTIN* was employed as a negative control locus. Values represent means ± SD (3 biological replicates). The experiments were performed twice with consistent results, and one representative experiment is illustrated. Asterisks indicate significant differences (*$P < 0.05$, **$P < 0.01$, ***$P < 0.001$; Student's *t*-test), "ns" denotes no statistical significance.

mutant (Fig. 8A; Supplementary Fig. S19). Concurrently, we evaluated the abundance of H3ac and observed a reduction in H3ac levels in WT plants compared to *brm-3* mutant. Subsequent analyses elucidated that this reduction stemmed from the inhibition of H3K14ac and H3K27ac levels within the *MYB41* promoter region in WT plants, unlike in *brm-3* mutant. This inhibitory mechanism ultimately curtailed the expression of *MYB41* (Fig. 8, B to D).

In summary, we can infer that BRM orchestrates the regulation of stomatal aperture and NO content in guard cells by suppressing the transcript levels of *MYB41*, thereby influencing the plant's resilience to drought stress.

A recent study highlighted that SWI3B and BRM, 2 integral subunits of the SWI/SNF chromatin–remodeling complex, establish direct interactions with the histone deacetylase HDA6 (At5g63110), resulting in the repression of transposons through modulation of DNA methylation and histone H3 acetylation levels (Yang et al. 2020; Li et al. 2022). In our study, we employed the *hda6* mutant line *axe1-5* (CS66153), which harbors a splicing mutation at the HDA6 splicing site and is derived from the Col-0 background (Murfett et al. 2001; Chen et al. 2010). Our ChIP assay using an anti-H3ac antibody on 14-d-old WT and *axe1-5* seedlings revealed a significant increase in H3 acetylation levels across the *MYB41* promoter in the *axe1-5* mutant (Fig. 9A). Additionally, an elevated *MYB41* expression was observed in the *axe1-5* mutant compared to WT (Fig. 9B). Further ChIP results confirmed the enrichment of HDA6 at the *MYB41* locus in WT plants, a pattern notably diminished in the *brm* mutant (Fig. 9C). These results suggest that BRM recruits its interactor HDA6 (Yang et al. 2020; Li et al. 2022), facilitating the removal of histone acetylation marks at the *pMYB41* to regulate *MYB41* transcript levels.

Synthesizing our collective findings, we propose a working model elucidating the role of MYB41 (Fig. 10). In WT plants, the MYB41 transcription factor recruits the chromatin remodeling ATPase, BRM, in the absence of ABA treatment. Subsequently, BRM engages HDA6, initiating histone deacetylation and thereby repressing *MYB41* expression. Conversely, in the *brm-3* mutant, H3K27me3 levels decrease, while H3ac, H3K14ac, and H3K27ac levels rise at the *MYB41* locus compared to WT (Fig. 8). Additionally, disruption of BRM in the *brm* mutant impedes the interaction between BRM and MYB41, preventing the recruitment of HDA6 to the *MYB41* promoter. This disruption results in elevated levels of H3ac, H3K14ac, and H3K27ac, ultimately activating *MYB41* (Fig. 10A).

Remarkably, in the presence of ABA accumulation, BRM undergoes phosphorylation-induced inactivation (Peirats-Llobet et al. 2016).

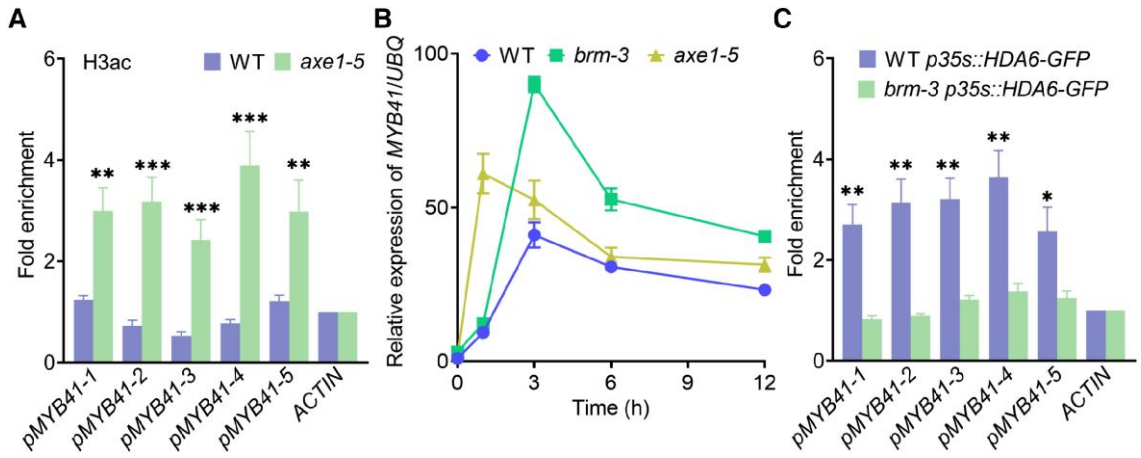

Figure 9. HDA6 involvement in ABA-mediated *MYB41* expression is BRM-dependent. **A)** Chromatin immunoprecipitation (ChIP)-qPCR analysis of H3 acetylation levels at the *MYB41* locus in wild-type (WT) and *axe1-5* seedlings cultured on 1/2 MS medium for 14 d. Relative enrichment was normalization to the internal control (*ACTIN*). The locations of the primers used for ChIP-qPCR are indicated in Fig. 4A. Values represent means ± SD (3 biological replicates). The experiments were performed twice with consistent results, and one representative experiment is shown. Asterisks indicate significant differences (**$P < 0.01$, ***$P < 0.001$; Student's *t*-test). **B)** Relative expression levels of *MYB41* in WT, *brm-3* and *axe-1-5* plants. Seven-day-old seedlings were treated with 0 μM abscisic acid (ABA [Control]) or 10 μM ABA for 1, 3, 6, and 12 h, followed by total RNA extraction. Data represent means ± SD of 3 independent experiments. Error bars are overlaid by symbols when not visible. **C)** Level of GFP-tagged HDA6 in *HDA6-GFP* and *brm3 HDA6-GFP* plants, and ChIP-qPCR analysis of HDA6-GFP enrichment at different regions of the *MYB41* locus in *HDA6-GFP* and *brm3 HDA6-GFP* plants, using an anti-GFP antibody. Relative enrichment was normalization to the internal control (*ACTIN*). Values represent means ± SD (3 biological replicates). The experiment was performed twice with consistent results, and one representative experiment is shown. Asterisks indicate significant differences (*$P < 0.05$, **$P < 0.01$; Student's *t*-test).

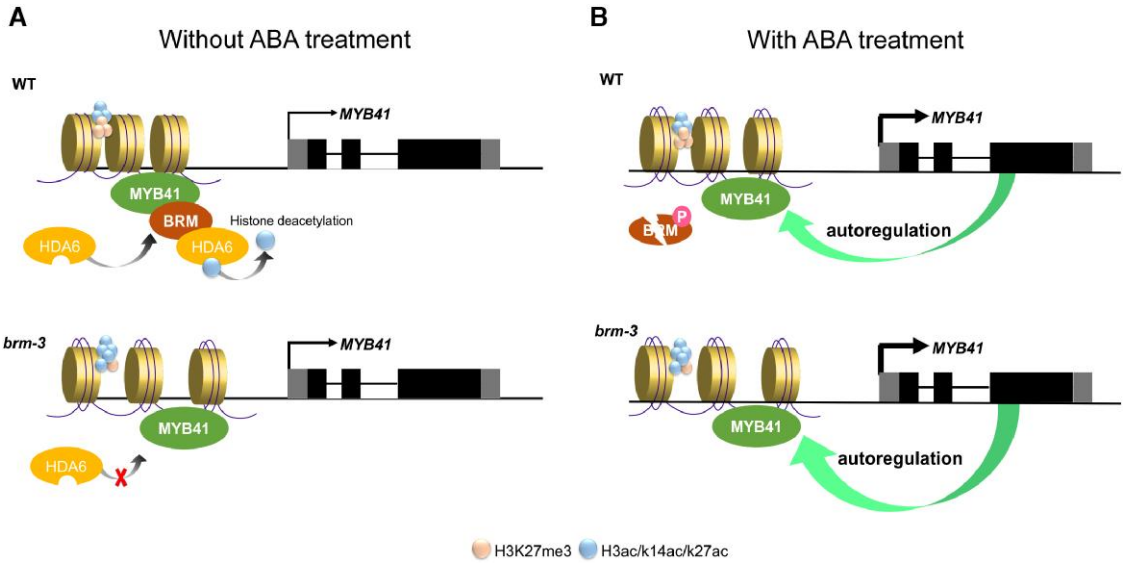

Figure 10. Autoregulation of the proposed MYB41-BRM model. **A)** Without abscisic acid (ABA) treatment, in wild-type (WT) plants, the chromatin remodeling ATPase BRM is recruited by the MYB41 transcription factor. Subsequently, HDA6 is recruited by BRM, enabling the mediation of histone deacetylation, resulting in reduced levels of H3ac, H3K14ac, and elevated levels of H3K27me3, ultimately repressing *MYB41* expression. In the *brm-3* mutant, due to the knockout of *BRM*, the interaction of BRM and MYB41 is disrupted, preventing the recruitment of HDA6 to the *MYB41* promoter. The altered chromatin landscape likely leads to increased levels of H3ac, H3K14ac, and H3K27ac, while H3K27me3 levels are reduced, resulting in the activation of *MYB41* expression. **B)** Upon ABA treatment, in WT, BRM becomes phosphorylated and inactive (Peirats-Llobet *et al.* 2016). This phosphorylation disrupts the interaction between BRM and MYB41. While inaction of the inhibition by BRM, ABA induces *MYB41* transcription and further activates *MYB41* transcription by its autoregulation. In the *brm-3* mutant, due to the knockout of *BRM*, without the inhibition by BRM and low H3K27me3 level at *pMYB41*, MYB41 autoregulation is enhanced, further boosting *MYB41* expression. The thickness of the black arrows indicates the expression levels of *MYB41*.

This inactivation probably weakens its ability to interact with MYB41, thereby releasing the inhibition by BRM. At the same time, ABA induces *MYB41* transcription, further activating *MYB41* transcription through its autoregulation. In the *brm-3* mutant, due to the knockout of *BRM*, without inhibition by BRM and low H3K27me3 level at *pMYB41*, MYB41 autoregulation is enhanced, further boosting *MYB41* expression (Fig. 10B). MYB41 positively affects ABA-mediated stomatal closure (Fig. 1). The elevated *MYB41* expression under ABA treatment results in a more closed stomatal aperture and greater drought tolerance, while

knockout of *MYBs* (*mybs*) results in a more open stomatal aperture and weaker drought tolerant (Figs. 1 and 2; Supplementary Fig. S3). The elevated *MYB41* expression in the *brm* mutants results in a more closed stomatal aperture and greater drought tolerance (Fig. 6; Supplementary Figs. S11 and S12).

Discussion

ABA serves as a central regulatory factor in plants' defense against various abiotic stresses, notably contributing to water balance through the intricate modulation of stomatal movement (Kim et al. 2010; Zhu 2016; Vishwakarma et al. 2017). Among the players in stomatal regulation, AtMYB60 and AtMYB96 serve as a pivotal driver of ABA-mediated stomatal modulation, effectively diminishing stomatal aperture and bolstering the plant's resilience to water scarcity (Cominelli et al. 2005; Seo et al. 2009). Intriguingly, the extent of MYB41's role in the regulation of water loss through the modulation of stomatal dynamics remains a subject largely unexplored in current literature.

In our study, *MYB41* exhibited the fastest and most robust transcriptional response to ABA treatment compared to its counterparts, namely *MYB74*, *MYB102*, *MYB9* and *MYB107* (Fig. 1A). The predominant accumulation of MYB41 in stomata further supports its potential involvement in stomatal regulation (Fig. 1B). While the presence of functionally redundant MYBs may partially compensate for MYB41's absence, our observations indicate that MYB41, in conjunction with MYB74 and MYB102, significantly contributes to the precise modulation of stomatal dynamics (Fig. 1; Supplementary Figs. S3 and S4).

Subsequently, our preliminary investigations offer intriguing insights into the potential autoregulation of *MYB41*—a positive feedback loop—in response to ABA-mediated desiccation. *MYB* knockout mutant exhibited a more open stomatal aperture, resulting in a higher water-loss rate and weakened drought tolerance compared to WT (Figs. 1C, 2, F and G, 3, and 4E). Moreover, we observed a substantial increase in *MYB41* promoter activity in the presence of its CDS, coupled with a notable decline in promoter activity within the 2 k to 1.5 k region—an observation hinting at the presence of pivotal regulatory motifs in this segment (Fig. 3B). Subsequent mutation analyses firmly establish the importance of this motif in governing *MYB41* promoter activity, evidenced by the marked reduction in promoter activity (Fig. 3, D and E). The culmination of our research efforts, encompassing EMSA and ChIP results, affirms a remarkable revelation: MYB41 directly engages with its own promoter region, specifically within the *pMYB41-1* region, effectively nurturing its self-expression (Fig. 4, A to C). This positive feedback loop assumes a vital role, empowering cells to deftly modulate *MYB41* expression levels, thereby enhancing sensitivity and efficacy in response to various environmental stresses.

Remarkably, our research revealed that BRM, an ABA signal repressor, mediates suppression of MYB41 autoregulation via epigenetic histone modification. Our initial investigations have unveiled a compelling facet—*MYB41* transcriptional levels surge anomalously in the *brm* mutants, both in the absence and presence of ABA treatment (Figs. 6, H and 7A). This striking observation underscores BRM's role as a regulator, effectively orchestrating a nuanced temporal modulation of *MYB41* transcription across diverse conditions. Subsequently, our study adeptly demonstrates the physical interaction between BRM and MYB41 through yeast 2-hybrid, BiFC, and pull-down assays (Fig. 5, A to F). Bioinformatical predictions and ChIP experiments unequivocally established BRM's direct binding to the *MYB41* promoter region (Fig. 7, B to D; Supplementary Fig. S18). Previous reports have highlighted BRM's association with histone modification, including H3K27me3 levels or H3K4me3 levels (Tie et al. 2012; Wu *et al.* 2012; Han *et al.* 2015; Yang *et al.* 2015; Zhao *et al.* 2015; Archacki *et al.* 2017; Zhang *et al.* 2017), and H3K9K14ac and H3K27ac levels through its recruitment of HDA6 (Sakamoto *et al.* 2018; Li *et al.* 2022). Here, we found that BRM bound to the *MYB41* promoter region, concurrent with an activation of H3K27me3 levels therein (Fig. 8A). In addition, the investigation into H3 acetylation levels revealed a consequential inhibition, further elucidated by probing H3K14ac and H3K27ac levels, ultimately culminating in a curbed expression of *MYB41* (Fig. 8, B to D). To decipher the intricacies of BRM's binding to the *MYB41* promoter, we performed ChIP analyses, revealing that the enrichment efficiency of *MYB41* in *brm-3 p35S:MYB41-GFP* outstripped that of WT *p35S:MYB41-GFP*, particularly within the *pMYB41-1* segment. This observation signifies BRM's competence in curbing MYB41's autoregulation (Fig. 7B). Intriguingly, the enrichment efficiency of *pMYB41-1* in *brm-1 pBRM:BRM-GFP* surpassed that in *trip-myb brm-1 pBRM:BRM-GFP*, implying that MYB41 can proficiently enlist BRM for a direct engagement with the *MYB41* promoter (Fig. 7, C and D).

The genetic data aligns with our proposed model. We accessed the phenotypes of stomatal movement, NO content, drought tolerance, seed germination and seedling root growth in WT, *brm*, *myb*, and *brm-myb* mutants. The *myb* mutants exhibited an ABA-insensitive phenotype (Fig. 2; Supplementary Figs. S2 to S10), while the *brm* mutants displayed an ABA-hypersensitive phenotype compared to WT (Fig. 6; Supplementary Figs. S11 to S13, and S15). Moreover, the *brm-3-trip-myb* or *myb74 myb102 brm-5* mutants exhibited a phenotype quite similar to the *trip-myb* or *myb74 myb102* mutants respectively, compared to WT (Fig. 6; Supplementary Figs. S13 and S15 and S16), indicating that these MYBs work downstream of BRM.

However, unlike the phenotype of *brm-3-trip-myb* or *myb74 myb102 brm-5* mutants in seed germination and seedling root growth (Supplementary Figs. S15 and S16), the phenotype of these 2 mutants in stomatal movement, NO accumulation, and drought tolerance falls within the intermediate range between the *trip-myb* or *myb74 myb102* and *brm-3* or *brm-5* mutants, respectively (Fig. 6; Supplementary Figs. S11 and S12). This suggests that other MYBs may work redundantly with MYB41, MYB74, and MYB102. The transcript levels of other members of MYB Subgroup 10–MYB9 and MYB39–were upregulated in the *brm-3* mutant, confirming the presence of functional redundancy (Supplementary Fig. S17). Further exploration is needed to elucidate the regulatory mechanism of these other MYBs in seed germination and seedling root growth or in stomatal movement, and drought tolerance, respectively.

Drought, a prominent global environmental challenge, emphasizes the critical need to unravel the molecular mechanisms that contribute to plants' resilience under drought stress. Our study holds profound significance, extending its impact to ecological conservation, sustainable food production, and comprehensive development. Ultimately, this research stands to positively influence both the global environment and human survival.

Materials and methods

Plant materials and growth conditions

Arabidopsis (*Arabidopsis thaliana*) T-DNA insertion mutants were obtained from the Arabidopsis Biological Resource Center. The mutant *myb102* (CS26067) was generated in the *Landsberg erecta*

(Ler) ecotype background. The other mutants, including *myb74* (SALK_073544C), *brm-3* (SALK_088462), *brm-5* (CS68980), *ost1-3* (SALK_008068), and *pER8GW:MYB41* (CS2104645) were generated in the WT (Col-0) ecotype background. The *pBRM:BRM-GFP brm-1* transgenic plants were previously described (Li et al. 2015), and seeds were kindly provided by Dr. Keqiang Wu's group from National Taiwan University. The following mutants were generated for this study using CRISPR-Cas9 technology: *myb41-6* (*myb41*), *myb41-30*, *myb41-58*, and *myb41 myb102* (*doub-myb*). The mutant *doub-myb* was crossed with *myb74* to generate the *myb41 myb74 myb102* (*trip-myb*), then the mutant *trip-myb* was crossed with *brm-3* to generate *brm-3 myb41 myb74 myb102* quadruple mutant. The mutant *myb74 myb102* was crossed with *brm-5* to generate the *myb74 myb102 brm-5* mutant; and the double mutant, *myb41 ost1-3* was generated by crossing *myb41* with *ost1-3*. Primers used for genotyping are presented in Supplementary Table S2. The seeds were surface sterilized with 75% (v/v) ethanol and stratified at 4 °C for 3 d under dark conditions and then were sown in 1/2 Murashige and Skoog (MS) medium containing 1% (w/v) sucrose and 0.8% (w/v) agar. The seedlings were subsequently transferred and sown in a potting mix of soil: vermiculite: perlite (3:1:1, v/v/v) and grown in plant growth chambers under 16-h-light/8-h-dark cycles (Long-day, LD) at 22 °C and 70% relative humidity. Fully expanded rosette leaves of 3-wk-old healthy plants were collected for use.

Generation of transgenic lines

To generate GUS-expressing transgenic lines (2 kb *pMYB41:GUS*, 1.5 kb *pMYB41:GUS*, and 2 kb-mut *pMYB41:GUS*), different fragments of the *MYB41* promoter were amplified by polymerase chain reaction (PCR). Each fragment was cloned into the modified pCAMBIA1300 binary vector, which includes both the GUS reporter gene and NOS terminator sequence. The constructs were transformed into WT or *trip-myb* backgrounds using the Agrobacterium (*Agrobacterium tumefaciens*)-mediated Arabidopsis floral dipping method (Clough and Bent 1998).

Total RNA extraction and RT-qPCR

Total RNA was extracted from 7-d-old seedlings using Trizol reagent (Invitrogen), and 1 μg of total RNA was used for first-strand cDNA synthesis with a Prime Script TM RT reagent Kit with gDNA eraser (TaKaRa). Quantitative RT-PCR (RT-qPCR) was performed using SYBR Premix Ex Taq II (TaKaRa) on an Applied Biosystems 7500 Fast real-time PCR system (Applied Biosystems). The PCR program included an initial denaturation step at 95 °C for 5 min, followed by 40 cycles of 30 s at 95 °C and 30 s at 60 °C and 30 s at 72 °C. Each sample was normalized using the housekeeping gene Ubiquitin 10 (UBQ) as an internal control. The gene-specific primer sets were listed in Supplementary Table S2. All PCRs were normalized using Ct value corresponding to the reference gene UBQ. Three technical replicates were performed for each sample and the expression level was calculated by the $2^{-\Delta\Delta Ct}$ method (Livak and Schmittgen 2001).

GUS staining and 4-methylumbelliferyl glucuronide assay

Two-week-old seedlings or leaves were immersed in GUS staining solution (0.5 mg/mL 5-bromo-4-chloro-3-indolyl-glucuronide, 20% (v/v) methanol, 0.01 M Tris–HCl, pH 7.0). After incubation at 37 °C overnight, the staining solution was removed, and samples were cleared by sequential changes of 75% (v/v) and 95% (v/v) ethanol. Photographed with a light microscope (Axio Zoom.V16, Zeiss).

4-Methylumbelliferyl glucuronide (MUG) assay was performed in T1 seedlings to study the regulation of promoter deletion conditions. The compound, MUG assays were performed as previously described with 4-methylumbelliferone (Sigma-Aldrich) being used as the standard, which upon hydrolysis produces the fluorescent 4-methylumbelliferone (4-MU). Standard curve was prepared using different concentrations of 4-MU (Jefferson et al. 1987). Protein concentration was determined using a Bradford reagent (Bradford 1976). In brief, at least 20 seedlings for each construct were pooled and harvested. Fluorescence was measured with 3 technical replicates and 3 biological replicates using separate T1 pools.

Stomatal aperture and density measurement

Soil-grown Arabidopsis (3-wk-old) were used for stomatal aperture and density measurements. Epidermis (epidermal strips) peeled from the abaxial surface of fully expanded leaves. The strips were preincubated at 22 °C in the light for 3 h in opening buffer (10 mM MES and 10 mM KCl, pH 6.15) under white light to promote stomatal opening before treatments (Distéfano et al. 2012). Subsequently, leaves or abaxial epidermal strips were treated with 10 μM ABA for 30 min. All chemicals were obtained from Sigma-Aldrich. After the treatments, the abaxial epidermis was peeled from the treated leaves. Epidermal strips for both the stomatal aperture and density measurement were imaged using a calibrated light microscope (Nikon Ni-E). The pore size of stomata was digitally calculated using the image analysis software Nikon. Aperture values represent the average ratio of width to length from 60 to 80 stomata measurements.

Drought stress tolerance and water-loss assays

Seven-day-old seedlings of both WT and mutants were transferred to soil for and allowed to grow for a period of 14 d, randomly placed in growth chambers and alternated every other day to ensure uniform environmental conditions, consistent with the parameters mentioned earlier. Prior to the drought experiment, all plants were thoroughly watered (saturated) during the night, but no further watering was provided throughout the assay, following the methodology outlined in a previous study (Xu et al. 2021). During the drought assay, all plants were randomly moved around once a day to avoid any bias of uneven light distribution or air flow within the cabinet that may impact water loss. Photographs were taken when the greatest difference in appearance was discerned between WT and mutant plants during the drought assay. For water-loss assays, leaves at the same developmental stage were excised from WT mutant plants that were grown under normal conditions. The detached leaves were placed on a laboratory bench and weighed at the designated times. The loss of fresh weight was calculated based on the initial weight of detached leaves. Water loss was presented as a percentage of fresh weight. The experiment was repeated 3 times.

Detection and quantification of NO

NO levels in stomata were detected with specific fluorescent 3-amino, 4-aminomethyl-2′,7′-difluorofluorescein diacetate DAF-FM-DA (Sigma-Aldrich), as described previously (Lv et al. 2022). Briefly, epidermal strips of 3-week-old Arabidopsis plants were incubated in the opening buffer for 3 h in the light and then treated with 10 μM ABA for 30 min. Next, the strips were incubated for 30 min with 10 μM DAF-FM-DA before washing in the opening

buffer 3 times to remove residual probe. Fluorescence was detected under a microscope (Nikon Ni-E) equipped with a charge-coupled device camera (excitation, 495 nm; acquisition, 515 nm). For quantification of fluorescence, the whole stomata areas of the micrographs were analyzed using the NIS-Elements BR4.60.00 software.

Yeast two-hybrid assay

Yeast 2-hybrid assay was performed as described in the manual of Matchmaker Gold Yeast Two-Hybrid Systems (Clontech). For the construction of the bait and prey, full-length and different deletion coding regions of BRM and MYB41 were fused into pGBKT7 (binding domain) and pGADT7 (activation domain) vectors, respectively. Then, the transfected yeast cells were grown on DDO medium (minimal media double dropouts, SD/-Leu/-Trp medium) for 3 d. Transformed colonies were dropped onto QDO medium (minimal media quadruple dropouts, SD/-Ade/-His/-Leu/-Trp medium) and cultured at 30 °C for 5 d, containing 4 mg/mL X-α-Gal (QDO/X) to test for possible interactions between BRM and MYB41 according to their growth status. The primers used for vector construction are listed in Supplementary Table S2.

In vitro pull-down assays

In vitro pull-down assays were performed as described (Zhao et al. 2015) with some modifications. The N-terminal fragment of BRM (BRM-DVII) was fused with the MBP-His tag and MYB41 was fused with the GST tag. GST or GST-MYB41 recombinant proteins were incubated with GST resin (GE Healthcare, USA) in a binding buffer (50 mM Tris, pH 7.4; 120 mM NaCl; 5% glycerol; 0.5% Nonidet P-40; 1 mM phenylmethylsulfonyl fluoride; and 1 mM β-mercaptoethanol) for 2 h at 4 °C, and were then collected and mixed with supernatant containing MBP-His-BRM-DVII protein, and incubated at 30 °C for 60 min. After being rinsed 5 times with washing buffer (50 mM Tris, pH 7.4, 120 mM NaCl, 5% glycerol, and 0.5% Nonidet P-40), the bound proteins were boiled in sodium dodecyl sulfate (SDS) sample buffer and subjected to SDS-polyacrylamide gel electrophoresis and immunoblotting.

Bimolecular fluorescence complementation (BiFC) analysis

Arabidopsis protoplast isolation and transformation were performed as described (Yoo et al. 2007). BiFC assays tested the interaction of BRM-N (in pSAT1-cCFP-C) with MYB41 (in pSAT1-cCFP-N) by co-transformation of pSAT1-cCFP-C/pSAT1-cCFP-N constructs into protoplasts (Waadt et al. 2008).

Electrophoretic mobility shift (EMSA) assay

EMSA analysis was performed as described (Ning et al. 2015) with some modifications. Four or 8 μg of purified MYB41 protein was incubated with 200 ng of promoter sequence obtained by PCR amplification in a binding buffer [25 mM HEPES (pH 7.6), 50 mM KCl, 0.1 mM EDTA, 12.5 mM $MgCl_2$, 1 mM DTT, 0.5% (w/v) BSA and 5% (w/v) glycerol] for 1 h at 25 °C. The binding mixture was loaded onto the 8% non-denaturing polyacrylamide gel at 100 V on ice for 1.5 h, and the binding DNA signals were detected by ethidium bromide staining.

Chromatin immunoprecipitation with quantitative PCR (ChIP–qPCR) assay

ChIP using Arabidopsis mesophyll protoplasts expressing MYB41 fused with a GFP tag was performed as previously described (Lee et al. 2017) with some modifications. About 100 μg plasmids were transformed into 2×10^7 protoplasts expressing MYB41-GFP were fixed in 1% formaldehyde (Sigma-Aldrich) for 10 min, and then crosslinking quenched with 2 M glycine (Sigma-Aldrich) for 5 min. Protoplasts were collected by centrifugation at 500×g for 2 min and washed twice with PBS buffer. The protoplast pellets were used to isolate nuclei and chromatin. ChIP using seedlings was performed as previously described (Yu et al. 2011) with modifications. Briefly, two grams of 14-d-old seedlings grown on MS agar was cross-linked with 1% formaldehyde and then ground into fine power with liquid nitrogen. The chromatin was extracted and then sheared to an average length of 500 bp by sonication. The chromatin was immunoprecipitated with specific antibodies including anti-GFP (Abcam, ab290), anti-H3K27me3 (Abcam, ab6002), anti-H3ac (Sigma-Aldrich, 06–599), anti-H3K14ac (Millipore, 07–353), and anti-H3K27ac (Millipore, 07–360). The precipitated DNAs were analyzed using RT-qPCR. Specifically, *pMYB41-1* refers to the promoter region from −1826 nt to −1691 nt, *pMYB41-2* refers to the promoter region from −1,532 nt to −1,401 nt, *pMYB41-3* refers to the promoter region from −1,393 nt to −1,264 nt, *pMYB41-4* refers to the promoter region from −1,250 nt to −1,100 nt, and *pMYB41-5* refers to the promoter region from −1,087 nt to −929 nt. The primers used for ChIP–qPCR are listed in Supplementary Table S2.

Dual-luciferase reporter assays

The AtMYB41 CDS was amplified from Arabidopsis cDNA and then transferred into the pGreen II 62-SK vector. The amplified 2 kb, 1.5 kb, 1.4 kb, 1.3 kb, 1.1 kb, and 0.5 kb promoter fragments upstream of the ATG start codon of the *MYB41* genes were transferred into the pGreen II 0800-LUC vector. Arabidopsis protoplasts were prepared for co-transfection with the effector and reporter constructs. After being cultured for 16 h under low light conditions, the LUC-to-GUS activity ratio was determined using the dual-luciferase reporter system following the manufacturer's instructions (Promega). The ratio of LUC to GUS indicates promoter activity. The primers used in this assay are listed in Supplementary Table S2. Three biological repeats were performed in this analysis.

Statistical analysis

The experimental data are presented as means with standard errors or standard deviations. For variance analysis, the Statistical Package for the Social Sciences (SPSS) was used to assess statistically significant differences ($P < 0.05$) based on Student's *t*-test or Tukey's test. Values at $P < 0.05$ were considered statistically significant.

Accession numbers

Sequence data from this article can be found in the public online database (https://www.arabidopsis.org/), under accession numbers: *AtMYB41* (At4g28110), *AtMYB74* (At4g05100), *AtMYB102* (At4g21440), *MYB9* (At5g16770), *MYB39* (At4g17785), *AtMYB107* (At3g02940), *BRM* (At2g46020), and *HDA6* (At5g63110).

Acknowledgments

We would like to thank the Arabidopsis Biological Resource Center for providing the T-DNA insertion mutants used in this study. We would like to express our sincere appreciation to Prof. Ligeng Ma, Prof. Legong Li, Prof. Liangyu Liu and Prof. Xiaoting Qi from Capital Normal University for their invaluable technical assistance and support. We also thank Prof. Min Zhang from Capital Normal University for generously providing the pCambia1300-GFP vector.

Author contributions

Y.He, Q.L., L.W., and L.G. designed the project. L.G., Y.C., and J.W. planned and performed the experiments. S.H., W.Z., X.Z., F.B., and Y.Hu provided assistance for experiments. L.G. wrote the manuscript with input from all authors. Y.He, L.W., L.L., and Q.L. revised the manuscript. All authors read and approved the final manuscript.

Supplementary data

The following materials are available in the online version of this article.

Supplementary Figure S1. *AtMYB41* expression in leaf veins.

Supplementary Figure S2. Genotype of the *myb41* and *myb102* mutants created by CRISPR-Cas9 technology.

Supplementary Figure S3. Stomatal aperture of different *myb* mutants.

Supplementary Figure S4. Water-loss rate of detached leaves of different *myb* mutants.

Supplementary Figure S5. Stomatal density of different *myb* mutants.

Supplementary Figure S6. Stomatal aperture of *myb41* and *ost1-3* mutants.

Supplementary Figure S7. Nitric oxide accumulation in guard cells of different *myb* mutants.

Supplementary Figure S8. Stomatal aperture and nitric oxide accumulation in guard cells of different time points.

Supplementary Figure S9. The *myb41*, *doub-myb*, and *trip-myb* mutants affect the expression of *NOA1*, *NIA1*, and *NIA2*.

Supplementary Figure S10. The *myb41*, *doub-myb*, and *trip-myb* mutants are insensitive to ABA.

Supplementary Figure S11. BRM inhibits NO accumulation and stomatal closure in guard cells.

Supplementary Figure S12. BRM affects plant drought resistance.

Supplementary Figure S13. Contrasting effects of *brm-5* and *myb* on Stomatal and NO accumulation.

Supplementary Figure S14. Overexpression of BRM inhibits NO accumulation and stomatal closure.

Supplementary Figure S15. The *brm-3* mutants are hypersensitive to ABA, and *trip-myb* reduces this sensitivity.

Supplementary Figure S16. The *brm-5* mutants are hypersensitive to ABA, and *myb41 and myb74* reduce this sensitivity.

Supplementary Figure S17. Relative expression levels of *MYB9*, *MYB39*, and *MYB107* in WT and *brm-3* plants.

Supplementary Figure S18. Searching for upstream factors for *MYB41* gene in Plant Regulomics.

Supplementary Figure S19. ChIP using Arabidopsis mesophyll protoplasts protein expression detection.

Supplementary Table S1. Upstream factors binding *MYB41* in *Arabidopsis thaliana*.

Supplementary Table S2. List of the primers used in this study.

Funding

This work was supported by the State Key Program of National Natural Science Foundation of China (31530006) and the Generate Program of National Natural Science Foundation of China (31970658) to Y.H., the Funding of Shihezi University (RCZK202468) to L.W., and the United States National Science Foundation (2238942) to L.L.

Conflict of interest statement. None declared.

Data availability

All data are available in the main text or the Supplementary supplementary materials. Materials are available from the corresponding author upon request.

References

Archacki R, Sarnowski TJ, Halibart-Puzio J, Brzeska K, Buszewicz D, Prymakowska-Bosak M, Koncz C, Jerzmanowski A. Genetic analysis of functional redundancy of BRM ATPase and ATSWI3C subunits of Arabidopsis SWI/SNF chromatin remodelling complexes. *Planta*. 2009:229(6):1281–1292. https://doi.org/10.1007/s00425-009-0915-5

Archacki R, Yatusevich R, Buszewicz D, Krzyczmonik K, Patryn J, Iwanicka-Nowicka R, Biecek P, Wilczynski B, Koblowska M, Jerzmanowski A, *et al.* Arabidopsis SWI/SNF chromatin remodeling complex binds both promoters and terminators to regulate gene expression. *Nucleic Acids Res*. 2017:45(6):3116–3129. https://doi.org/10.1093/nar/gkw1273

Barros R, da Costa LT, Pinto-de-Sousa J, Duluc I, Freund JN, David L, Almeida R. CDX2 autoregulation in human intestinal metaplasia of the stomach: impact on the stability of the phenotype. *Gut*. 2011:60(3):290–298. https://doi.org/10.1136/gut.2010.222323

Bateman E. Autoregulation of eukaryotic transcription factors. *Prog Nucleic Acid Res Mol Biol*. 1998:60:133–168. https://doi.org/10.1016/S0079-6603(08)60892-2

Bradford MM. A rapid and sensitive method for the quantitation of microgram quantities of protein utilizing the principle of protein-dye binding. *Anal Biochem*. 1976:72(1–2):248–254. https://doi.org/10.1016/0003-2697(76)90527-3

Carrier TA, Keasling JD. Investigating autocatalytic gene expression systems through mechanistic modeling. *J Theor Biol*. 1999:201(1):25–36. https://doi.org/10.1006/jtbi.1999.1010

Chen LT, Luo M, Wang YY, Wu K. Involvement of Arabidopsis histone deacetylase HDA6 in ABA and salt stress response. *J Exp Bot*. 2010:61(12):3345–3353. https://doi.org/10.1093/jxb/erq154

Chen X, Wang Y, Feng T, Yi M, Zhang X, Zhou D. The overshoot and phenotypic equilibrium in characterizing cancer dynamics of reversible phenotypic plasticity. *J Theor Biol*. 2016:390:40–49. https://doi.org/10.1016/j.jtbi.2015.11.008

Cho EJ, Choi SH, Kim JH, Kim JE, Lee MH, Chung BY, Woo HR, Kim JH. A mutation in plant-specific SWI2/SNF2-like chromatin-remodeling proteins, DRD1 and DDM1, delays leaf senescence in *Arabidopsis thaliana*. *PLoS One*. 2016:11(1):e0146826. https://doi.org/10.1371/journal.pone.0146826

Claeys Bouuaert C, Lipkow K, Andrews SS, Liu D, Chalmers R. The autoregulation of a eukaryotic DNA transposon. *Elife*. 2013:2:e00668. https://doi.org/10.7554/eLife.00668

Clough SJ, Bent AF. Floral dip: a simplified method for *Agrobacterium*-mediated transformation of *Arabidopsis thaliana*. *Plant J*. 1998:16(6):735–743. https://doi.org/10.1046/j.1365-313x.1998.00343.x

Cominelli E, Galbiati M, Vavasseur A, Conti L, Sala T, Vuylsteke M, Leonhardt N, Dellaporta SL, Tonelli C. A guard-cell-specific MYB transcription factor regulates stomatal movements and plant drought tolerance. *Curr Biol*. 2005:15(13):1196–1200. https://doi.org/10.1016/j.cub.2005.05.048

Cominelli E, Sala T, Calvi D, Gusmaroli G, Tonelli C. Over-expression of the Arabidopsis *AtMYB41* gene alters cell expansion and leaf surface permeability. *Plant J*. 2008:53(1):53–64. https://doi.org/10.1111/j.1365-313X.2007.03310.x

Cramer GR, Urano K, Delrot S, Pezzotti M, Shinozaki K. Effects of abiotic stress on plants: a systems biology perspective. *BMC Plant Biol*. 2011:11(1):163. https://doi.org/10.1186/1471-2229-11-163

Daneva A, Gao Z, Van Durme M, Nowack MK. Functions and regulation of programmed cell death in plant development. *Annu Rev Cell Dev Biol*. 2016:32(1):441–468. https://doi.org/10.1146/annurev-cellbio-111315-124915

Distéfano AM, Scuffi D, García-Mata C, Lamattina L, Laxalt AM. Phospholipase Dδ is involved in nitric oxide-induced stomatal closure. *Planta*. 2012:236(6):1899–1907. https://doi.org/10.1007/s00425-012-1745-4

Dubos C, Stracke R, Grotewold E, Weisshaar B, Martin C, Lepiniec L. MYB transcription factors in Arabidopsis. *Trends Plant Sci*. 2010:15-(10):573–581. https://doi.org/10.1016/j.tplants.2010.06.005

Efroni I, Han SK, Kim HJ, Wu MF, Steiner E, Birnbaum KD, Hong JC, Eshed Y, Wagner D. Regulation of leaf maturation by chromatin-mediated modulation of cytokinin responses. *Dev Cell*. 2013:24(4):438–445. https://doi.org/10.1016/j.devcel.2013.01.019

Espley RV, Brendolise C, Chagné D, Kutty-Amma S, Green S, Volz R, Putterill J, Schouten HJ, Gardiner SE, Hellens RP, *et al*. Multiple repeats of a promoter segment causes transcription factor autoregulation in red apples. *Plant Cell*. 2009:21(1):168–183. https://doi.org/10.1105/tpc.108.059329

Farrona S, Hurtado L, Bowman JL, Reyes JC. The *Arabidopsis thaliana* SNF2 homolog AtBRM controls shoot development and flowering. *Development*. 2004:131(20):4965–4975. https://doi.org/10.1242/dev.01363

Gan L, Wu X, Zhong Y. Exogenously applied nitric oxide enhances the drought tolerance in hulless barley. *Plant Prod Sci*. 2015:18(1):52–56. https://doi.org/10.1626/pps.18.52

Garcia-Mata C, Lamattina L. Abscisic acid, nitric oxide and stomatal closure - is nitrate reductase one of the missing links? *Trends Plant Sci*. 2003:8(1):20–26. https://doi.org/10.1016/S1360-1385(02)00009-2

Han SK, Sang Y, Rodrigues A, Biol F, Wu MF, Rodriguez PL, Wagner D. The SWI2/SNF2 chromatin remodeling ATPase BRAHMA represses abscisic acid responses in the absence of the stress stimulus in Arabidopsis. *Plant Cell*. 2012:24(12):4892–4906. https://doi.org/10.1105/tpc.112.105114

Han SK, Wu MF, Cui SJ, Wagner D. Roles and activities of chromatin remodeling ATPases in plants. *Plant J*. 2015:83(1):62–77. https://doi.org/10.1111/tpj.12877

Hoang MHT, Nguyen XC, Lee K, Kwon YS, Pham HTT, Park HC, Yun D-J, Lim CO, Chung WS. Phosphorylation by AtMPK6 is required for the biological function of AtMYB41 in Arabidopsis. *Biochem Biophys Res Commun*. 2012:422(1):181–186. https://doi.org/10.1016/j.bbrc.2012.04.137

Hurtado L, Farrona S, Reyes JC. The putative SWI/SNF complex subunit BRAHMA activates flower homeotic genes in *Arabidopsis thaliana*. *Plant Mol Biol*. 2006:62(1–2):291–304. https://doi.org/10.1007/s11103-006-9021-2

Jefferson RA, Kavanagh TA, Bevan MW. GUS fusions: beta-glucuronidase as a sensitive and versatile gene fusion marker in higher plants. *EMBO J*. 1987:6(13):3901–3907. https://doi.org/10.1002/j.1460-2075.1987.tb02730.x

Jiang C-K, Rao G-Y. Insights into the diversification and evolution of R2R3-MYB transcription factors in plants. *Plant Physiol*. 2020:183(2):637–655. https://doi.org/10.1104/pp.19.01082

Kang Y, Gu C, Yuan L, Wang Y, Zhu Y, Li X, Luo Q, Xiao J, Jiang D, Qian M, *et al*. Flexibility and symmetry of prokaryotic genome rearrangement reveal lineage-associated core-gene-defined genome organizational frameworks. *mBio*. 2014:5(6):e01867. https://doi.org/10.1128/mBio.01867-14

Kim TH, Bohmer M, Hu H, Nishimura N, Schroeder JI. Guard cell signal transduction network: advances in understanding abscisic acid, CO_2, and ca^{2+} signaling. *Annu Rev Plant Biol*. 2010:61(1):561–591. https://doi.org/10.1146/annurev-arplant-042809-112226

Kosma DK, Murmu J, Razeq FM, Santos P, Bourgault R, Molina I, Rowland O. AtMYB41 activates ectopic suberin synthesis and assembly in multiple plant species and cell types. *Plant J*. 2014:80(2):216–229. https://doi.org/10.1111/tpj.12624

Lee JH, Jin S, Kim SY, Kim W, Ahn JH. A fast, efficient chromatin immunoprecipitation method for studying protein-DNA binding in *Arabidopsis* mesophyll protoplasts. *Plant Methods*. 2017:13(1):42. https://doi.org/10.1186/s13007-017-0192-4

Li C, Chen C, Gao L, Yang S, Nguyen V, Shi X, Siminovitch K, Kohalmi SE, Huang S, Wu K, *et al*. The Arabidopsis SWI2/SNF2 chromatin remodeler BRAHMA regulates polycomb function during vegetative development and directly activates the flowering repressor gene SVP. *PLoS Genet*. 2015:11(1):e1004944. https://doi.org/10.1371/journal.pgen.1004944

Li T, Zhang R, Satheesh V, Wang P, Ma G, Guo J, An GY, Lei M. The chromatin remodeler BRAHMA recruits HISTONE DEACETYLASE6 to regulate root growth inhibition in response to phosphate starvation in *Arabidopsis*. *J Integr Plant Biol*. 2022:64(12):2314–2326. https://doi.org/10.1111/jipb.13345

Lim J, Lim CW, Lee SC. Role of pepper MYB transcription factor CaDIM1 in regulation of the drought response. *Front Plant Sci*. 2022:13:1028392. https://doi.org/10.3389/fpls.2022.1028392

Lippold F, Sanchez DH, Musialak M, Schlereth A, Scheible WR, Hincha DK, Udvardi MK. Atmyb41 regulates transcriptional and metabolic responses to osmotic stress in Arabidopsis. *Plant Physiol*. 2009:149(4):1761–1772. https://doi.org/10.1104/pp.108.134874

Livak KJ, Schmittgen TD. Analysis of relative gene expression data using real-time quantitative PCR and the 2(-Delta Delta C(T)) method. *Methods*. 2001:25(4):402–408. https://doi.org/10.1006/meth.2001.1262

Lv Q, Han S, Wang L, Xia J, Li P, Hu R, Wang J, Gao L, Chen Y, Wang Y, *et al*. TEB/POLQ plays dual roles in protecting Arabidopsis from NO-induced DNA damage. *Nucleic Acids Res*. 2022:50(12):6820–6836. https://doi.org/10.1093/nar/gkac469

Ma D, Constabel CP. MYB repressors as regulators of phenylpropanoid metabolism in plants. *Trends Plant Sci*. 2019:24(3):275–289. https://doi.org/10.1016/j.tplants.2018.12.003

Majeed S, Nawaz F, Naeem M, Ashraf MY, Ejaz S, Ahmad KS, Tauseef S, Farid G, Khalid I, Mehmood K. Nitric oxide regulates water status and associated enzymatic pathways to inhibit nutrients imbalance in maize (*Zea mays L.*) under drought stress. *Plant Physiol Biochem*. 2020:155:147–160. https://doi.org/10.1016/j.plaphy.2020.07.005

Murfett J, Wang XJ, Hagen G, Guilfoyle TJ. Identification of Arabidopsis histone deacetylase HDA6 mutants that affect transgene expression. *Plant Cell*. 2001:13(5):1047–1061. https://doi.org/10.1105/tpc.13.5.1047

Mustilli A-C, Merlot S, Vavasseur A, Fenzi F, Giraudat J. Arabidopsis OST1 protein kinase mediates the regulation of stomatal aperture by abscisic acid and acts upstream of reactive oxygen species production. *Plant Cell*. 2002:14(12):3089–3099. https://doi.org/10.1105/tpc.007906

Neill S, Barros R, Bright J, Desikan R, Hancock J, Harrison J, Morris P, Ribeiro D, Wilson I. Nitric oxide, stomatal closure, and abiotic stress. *J Exp Bot*. 2008:59(2):165–176. https://doi.org/10.1093/jxb/erm293

Ning YQ, Ma ZY, Huang HW, Mo H, Zhao TT, Li L, Cai T, Chen S, Ma L, He XJ. Two novel NAC transcription factors regulate gene expression and flowering time by associating with the histone

demethylase JMJ14. *Nucleic Acids Res*. 2015:43(3):1469–1484. https://doi.org/10.1093/nar/gku1382

Ohgishi M, Oka A, Morelli G, Ruberti I, Aoyama T. Negative autoregulation of the *Arabidopsis* homeobox gene *ATHB-2*. *Plant J*. 2001:25(4):389–398. https://doi.org/10.1046/j.1365-313x.2001.00966.x

Peirats-Llobet M, Han SK, Gonzalez-Guzman M, Jeong CW, Rodriguez L, Belda-Palazon B, Wagner D, Rodriguez PL. A direct link between abscisic acid sensing and the chromatin-remodeling ATPase BRAHMA via core ABA signaling pathway components. *Mol Plant*. 2016:9(1):136–147. https://doi.org/10.1016/j.molp.2015.10.003

Richter R, Kinoshita A, Vincent C, Martinez-Gallegos R, Gao H, van Driel AD, Hyun Y, Mateos JL, Coupland G. Floral regulators FLC and SOC1 directly regulate expression of the B3-type transcription factor TARGET OF FLC AND SVP 1 at the Arabidopsis shoot apex via antagonistic chromatin modifications. *Plos Genet*. 2019:15(4):e1008065. https://doi.org/10.1371/journal.pgen.1008065

Sakamoto T, Tsujimoto-Inui Y, Sotta N, Hirakawa T, Matsunaga TM, Fukao Y, Matsunaga S, Fujiwara T. Proteasomal degradation of BRAHMA promotes boron tolerance in Arabidopsis. *Nat Commun*. 2018:9(1):5285. https://doi.org/10.1038/s41467-018-07393-6

Sarnowska E, Gratkowska DM, Sacharowski SP, Cwiek P, Tohge T, Fernie AR, Siedlecki JA, Koncz C, Sarnowski TJ. The role of SWI/SNF chromatin remodeling complexes in hormone crosstalk. *Trends Plant Sci*. 2016:21(7):594–608. https://doi.org/10.1016/j.tplants.2016.01.017

Seo PJ, Xiang F, Qiao M, Park JY, Lee YN, Kim SG, Lee YH, Park WJ, Park CM. The MYB96 transcription factor mediates abscisic acid signaling during drought stress response in Arabidopsis. *Plant Physiol*. 2009:151(1):275–289. https://doi.org/10.1104/pp.109.144220

Shen C, Zhang Y, Li Q, Liu S, He F, An Y, Zhou Y, Liu C, Yin W, Xia X. *PdGNC* confers drought tolerance by mediating stomatal closure resulting from NO and H_2O_2 production via the direct regulation of *PdHXK1* expression in *Populus*. *New Phytol*. 2021:230(5):1868–1882. https://doi.org/10.1111/nph.17301

Shukla V, Han JP, Cleard F, Lefebvre-Legendre L, Gully K, Flis P, Berhin A, Andersen TG, Salt DE, Nawrath C, *et al*. Suberin plasticity to developmental and exogenous cues is regulated by a set of MYB transcription factors. *Proc Natl Acad Sci U S A*. 2021:118(39):e2101730118. https://doi.org/10.1073/pnas.2101730118

Stracke R, Werber M, Weisshaar B. The R2R3-MYB gene family in Arabidopsis thaliana. *Curr Opin Plant Biol*. 2001:4(5):447–456. https://doi.org/10.1016/S1369-5266(00)00199-0

Tang X, Hou A, Babu M, Nguyen V, Hurtado L, Lu Q, Reyes JC, Wang A, Keller WA, Harada JJ, *et al*. The Arabidopsis BRAHMA chromatin-remodeling ATPase is involved in repression of seed maturation genes in leaves. *Plant Physiol*. 2008:147(3):1143–1157. https://doi.org/10.1104/pp.108.121996

Thouly C, Le Masson M, Lai X, Carles CC, Vachon G. Unwinding BRAHMA functions in plants. *Genes (Basel)*. 2020:11(1):90. https://doi.org/10.3390/genes11010090

Tie F, Banerjee R, Conrad PA, Scacheri PC, Harte PJ. Histone demethylase UTX and chromatin remodeler BRM bind directly to CBP and modulate acetylation of histone H3 lysine 27. *Mol Cell Biol*. 2012:32(12):2323–2334. https://doi.org/10.1128/MCB.06392-11

Vishwakarma K, Upadhyay N, Kumar N, Yadav G, Singh J, Mishra RK, Kumar V, Verma R, Upadhyay RG, Pandey M, *et al*. Abscisic acid signaling and abiotic stress tolerance in plants: a review on current knowledge and future prospects. *Front Plant Sci*. 2017:8:161. https://doi.org/10.3389/fpls.2017.00161

Waadt R, Manalansan B, Rauniyar N, Munemasa S, Booker MA, Brandt B, Waadt C, Nusinow DA, Kay SA III, Kunz HH, *et al*. Identification of open stomata1-interacting proteins reveals interactions with sucrose non-fermenting1-related protein kinases2 and with type 2A protein phosphatases that function in abscisic acid responses. *Plant Physiol*. 2015:169(1):760–779. https://doi.org/10.1104/pp.15.00575

Waadt R, Schmidt LK, Lohse M, Hashimoto K, Bock R, Kudla J. Multicolor bimolecular fluorescence complementation reveals simultaneous formation of alternative CBL/CIPK complexes *in planta*. *Plant J*. 2008:56(3):505–516. https://doi.org/10.1111/j.1365-313X.2008.03612.x

Wagner D, Meyerowitz EM. SPLAYED, a novel SWI/SNF ATPase homolog, controls reproductive development in Arabidopsis. *Curr Biol*. 2002:12(2):85–94. https://doi.org/10.1016/S0960-9822(01)00651-0

Wang Y, He S. Inference on autoregulation in gene expression with variance-to-mean ratio. *J Math Biol*. 2023:86(5):87. https://doi.org/10.1007/s00285-023-01924-6

Wilson ID, Neill SJ, Hancock JT. Nitric oxide synthesis and signalling in plants. *Plant Cell Environ*. 2008:31(5):622–631. https://doi.org/10.1111/j.1365-3040.2007.01761.x

Wu MF, Sang Y, Bezhani S, Yamaguchi N, Han SK, Li ZT, Su YH, Slewinski TL, Wagner D. SWI2/SNF2 chromatin remodeling ATPases overcome polycomb repression and control floral organ identity with the LEAFY and SEPALLATA3 transcription factors. *Proc Natl Acad Sci U S A*. 2012:109(9):3576–3581. https://doi.org/10.1073/pnas.1113409109

Xu Y, Guo C, Zhou B, Li C, Wang H, Zheng B, Ding H, Zhu Z, Peragine A, Cui Y, *et al*. Regulation of vegetative phase change by SWI2/SNF2 chromatin remodeling ATPase BRAHMA. *Plant Physiol*. 2016:172(4):2416–2428. https://doi.org/10.1104/pp.16.01588

Xu H, Liu P, Wang C, Wu S, Dong C, Lin Q, Sun W, Huang B, Xu M, Tauqeer A, *et al*. Transcriptional networks regulating suberin and lignin in endodermis link development and ABA response. *Plant Physiol*. 2022:190(2):1165–1181. https://doi.org/10.1093/plphys/kiac298

Xu B, Long Y, Feng X, Zhu X, Sai N, Chirkova L, Betts A, Herrmann J, Edwards EJ, Okamoto M, *et al*. GABA signalling modulates stomatal opening to enhance plant water use efficiency and drought resilience. *Nat Commun*. 2021:12(1):1952. https://doi.org/10.1038/s41467-021-21694-3

Yan J, Tsuichihara N, Etoh T, Iwai S. Reactive oxygen species and nitric oxide are involved in ABA inhibition of stomatal opening. *Plant Cell Environ*. 2007:30(10):1320–1325. https://doi.org/10.1111/j.1365-3040.2007.01711.x

Yang SG, Li CL, Zhao LM, Gao SJ, Lu JX, Zhao ML, Chen CY, Liu XC, Luo M, Cui YH, *et al*. The Arabidopsis SWI2/SNF2 chromatin remodeling ATPase BRAHMA targets directly to PINs and is required for root stem cell niche maintenance. *Plant Cell*. 2015:27(6):1670–1680. https://doi.org/10.1105/tpc.15.00091

Yang J, Yuan LY, Yen MR, Zheng F, Ji RJ, Peng T, Gu DC, Yang SG, Cui YH, Chen PY, *et al*. SWI3B and HDA6 interact and are required for transposon silencing in *Arabidopsis*. *Plant J*. 2020:102(4):809–822. https://doi.org/10.1111/tpj.14666

Yoo SD, Cho YH, Sheen J. Arabidopsis mesophyll protoplasts: a versatile cell system for transient gene expression analysis. *Nat Protoc*. 2007:2(7):1565–1572. https://doi.org/10.1038/nprot.2007.199

Yu X, Li L, Zola J, Aluru M, Ye H, Foudree A, Guo H, Anderson S, Aluru S, Liu P, *et al*. A brassinosteroid transcriptional network revealed by genome-wide identification of BESI target genes in *Arabidopsis thaliana*. *Plant J*. 2011:65(4):634–646. https://doi.org/10.1111/j.1365-313X.2010.04449.x

Zhang D, Li Y, Zhang X, Zha P, Lin R. The SWI2/SNF2 chromatin-remodeling ATPase BRAHMA regulates chlorophyll biosynthesis in Arabidopsis. *Mol Plant*. 2017:10(1):155–167. https://doi.org/10.1016/j.molp.2016.11.003

Zhao M, Yang S, Chen CY, Li C, Shan W, Lu W, Cui Y, Liu X, Wu K. Arabidopsis BREVIPEDICELLUS interacts with the SWI2/SNF2 chromatin remodeling ATPase BRAHMA to regulate KNAT2 and KNAT6 expression in control of inflorescence architecture. *PLoS Genet*. 2015:11(3):e1005125. https://doi.org/10.1371/journal.pgen.1005125

Zhu JK. Abiotic stress signaling and responses in plants. *Cell*. 2016:167(2):313–324. https://doi.org/10.1016/j.cell.2016.08.029

Zhu C, Perry SE. Control of expression and autoregulation of *AGL15*, a member of the MADS-box family. *Plant J*. 2005:41(4):583–594. https://doi.org/10.1111/j.1365-313X.2004.02320.x